

Parameter-optimal unitary synthesis with flag decompositions

Korbinian Kottmann, David Wierichs, Guillermo Alonso-Linaje, and Nathan Killoran
Xanadu, Toronto, ON, M5G 2C8, Canada

We introduce the *flag decomposition* as a central tool for unitary synthesis. It lets us carve out a diagonal unitary with 2^n degrees of freedom in such a way that the remaining *flag circuit* is parametrized by the optimal number of $4^n - 2^n$ rotations. This enables us to produce parameter-optimal quantum circuits for generic unitaries and matrix product state preparation. Our approach improves upon the state of the art, both when compiling down to the {Clifford + Rot} gate set with what we call *selective de-multiplexing*, and when using phase gradient resource states together with quantum arithmetic to implement multiplexed rotations. All of our synthesis methods are efficiently implementable in terms of recursive Cartan decompositions realized by standard linear algebra routines, making them applicable to all practically relevant system sizes.

I. INTRODUCTION

Unitary synthesis is an important subroutine in quantum compilation. It allows us to decompose arbitrary matrices of modest size into a sequence of gates that can be executed on a quantum computer. Leading techniques for (numerically) exact unitary synthesis are based on recursive Cartan decompositions [1–9], including the widely-used quantum Shannon decomposition (QSD) [1] and most advanced variant thereof [8]. These techniques have been developed with a focus on minimizing the required number of static entanglers like CNOT or CZ gates. However, non-Clifford gates such as T and Toffoli gates dominate the cost in fault-tolerant quantum computing (FTQC) [10, 11].

We revisit unitary synthesis from the perspective of minimizing parametrized rotation gates, which are the main contributors of non-Clifford gates. Each rotation gate can be either discretized into a series of {Clifford + T} operations [12–15], or realized via a combination of phase gradient resource states, quantum read-only memory (QROM) [16], and bit-wise quantum addition using Toffoli gates [17]¹. We develop unitary synthesis schemes that improve upon the best known resource counts for either decomposition strategy. An overview of the methods is provided in Fig. 1. The crucial ingredient is the parameter optimality, which is unlocked by the *flag decomposition*. This decomposition lets us split a unitary V into a diagonal operator Δ (including a global phase) and its “remainder” \mathbb{V} in a parameter-optimal fashion:

$$V_{4^n} = \mathbb{V}_{4^n - 2^n} \Delta_{2^n}$$

The diagram shows a quantum circuit with two horizontal lines representing qubits. On the left, a rectangular box labeled V_{4^n} has two input lines on the left and two output lines on the right. This is followed by an equals sign. To the right of the equals sign, there are two boxes in series. The first box is labeled $\mathbb{V}_{4^n - 2^n}$ and has two input lines on the left and two output lines on the right. The second box is labeled Δ_{2^n} and has two input lines on the left and two output lines on the right. The output lines of the second box are connected to the output lines of the first box.

The remainder \mathbb{V} of the unitary lives on a so-called complete flag manifold of dimension $4^n - 2^n$, complementing the diagonal gate that has 2^n parameters, as indicated by the subscripts in the circuit diagram. Thus, the optimum of 4^n parameters² for general unitary matrices is maintained. The elements of the (complete) flag manifold are equivalence classes, where equivalence is defined as equality up to left multiplication with a diagonal phase matrix. The particular representative of each class will be fixed through the decomposition of the flag circuit itself, which we construct recursively from the two known base cases for one and two qubits in Sec. III. It turns out that the resulting circuit is equivalent to an old result in [18, Fig. 3] that already achieved parameter-optimality via recursive cosine-sine decompositions (CSDs) but has been underappreciated in the literature since. The flag decomposition is a valid unitary synthesis scheme on its own and well-suited for the phase gradient decomposition, as discussed in Sec. III. Further, we use it as a subroutine in Sec. IV to derive *selective de-multiplexing* (SDM), a parameter-optimal decomposition that builds on the QSD and improves upon the CNOT gate count compared to [18, 19] (see Tab. I).

These parameter-optimal unitary synthesis schemes have direct implications for matrix product state (MPS) preparation, which is a crucial subroutine in many quantum algorithms [16, 20, 21]. There is a wide variety of preparation algorithms for MPS of different flavors [22–27]. In these preparation algorithms, the crucial subroutine that determines the overall cost of the circuit is unitary synthesis. In Sec. V, we tailor our synthesis techniques to become parameter-optimal with respect to the manifold spanned by the MPS matrices. In particular, we ensure that the reductions due to the isometric properties of MPS matrices, as well as the gauge freedom of MPS, is respected by the constructed circuits. We do this specifically for the MPS preparation scheme from [22], but note that the employed tricks apply to any MPS preparation scheme. Additionally, the reductions in the flag decom-

¹ We refer to this as the phase gradient decomposition (see Sec. III A for details) and note that this approach is sometimes also simply referred to as QROM in the literature.

² We consider the full unitary group $U(2^n)$, including a global phase, throughout this manuscript.

positions together with the optimizations for the MPS preparation circuits lead to improvements over the currently best-known quantum resources in terms of Toffoli gates in [21] when targeting phase gradient decompositions.

Implementations of all our synthesis techniques using SciPy [28] and PennyLane [29] can be found in [30].

II. RESULTS OVERVIEW

We derive the flag decomposition and use it to design parameter-optimal unitary synthesis methods. As indicated in Fig. 1, we differentiate two distinct decomposition methods:

- {Clifford + Rot} decomposition: Decomposing the circuit skeleton into Clifford gates and rotations.
- Phase gradient decomposition: Decomposing the circuit skeleton into a QROM and adders using many auxiliary qubits and a reusable phase gradient resource state.

We tailor our schemes to each decomposition method for general-purpose unitary synthesis. Further, we adapt the optimized synthesis circuits to MPS preparation to optimally take advantage of the inherent reduced dimensionality of the tensors in an MPS. These careful design choices lead to improvements upon the best known gate counts in all cases considered in Fig. 1. We continue below by providing an overview of the results for the two decomposition schemes and MPS preparation.

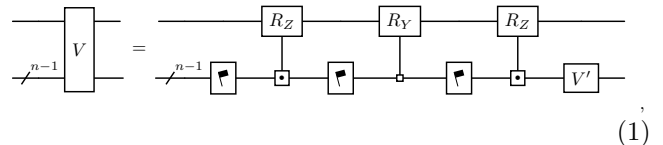
A. {Clifford + Rot} decomposition

For noisy intermediate-scale quantum computing (NISQ), where CNOT gates are the main contributors to noise and therefore the costliest resource, the quantum Shannon decomposition (QSD) [1] and variants thereof like the Block-ZXZ decomposition [8] provide the best unitary synthesis technique with the lowest CNOT gate count (see Tab. I).

For FTQC, we prioritize optimality in terms of the number of parametrized rotation gates. This was already achieved by an underappreciated decomposition in 2004 [19], using a recursive cosine-sine decomposition (CSD). In terms of CNOT cost, the best QSD variant has a leading-order factor of $\frac{22}{48}4^n$ CNOTs as indicated in Tab. I, whereas [19] has a leading-order factor of $\frac{1}{2}4^n$ CNOTs (see App. C). Hence, [19] is parameter-optimal while at the same time being only $\frac{1}{24}4^n$ away from the best-known CNOT count.

We improve upon this result by introducing what we call selective de-multiplexing (SDM) with the resources indicated in Tab. I. It provides the lowest CNOT count while at the same time being parameter-optimal.

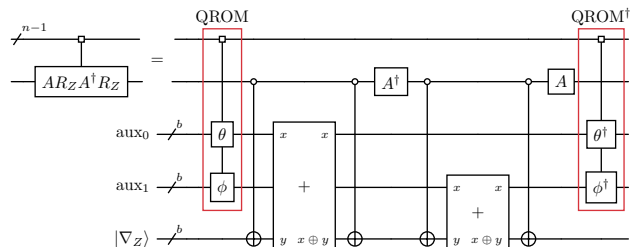
The resulting SDM circuit has the following recursive structure,



where each \square indicates the reduction of a $(n-1)$ -qubit unitary to the so-called complete flag manifold with $4^{n-1} - 2^{n-1}$ parameters, making the circuit overall parameter-optimal. The multiplexer node with a dot denotes a symmetrized multiplexer decomposition that removes one entangling gate; see Eq. (29). The full derivation with all optimization tricks to reduce the CNOT count is provided in Sec. IV. A prerequisite of selective de-multiplexing is the flag decomposition, which we derive in Sec. III. Its dense multiplexer structure is well-suited for phase gradient decompositions, as we discuss next.

B. Phase gradient decomposition

We consider the phase gradient decomposition that realizes the multiplexer of two consecutive Z rotation gates, potentially with an intermediate basis change given by A and A^\dagger :

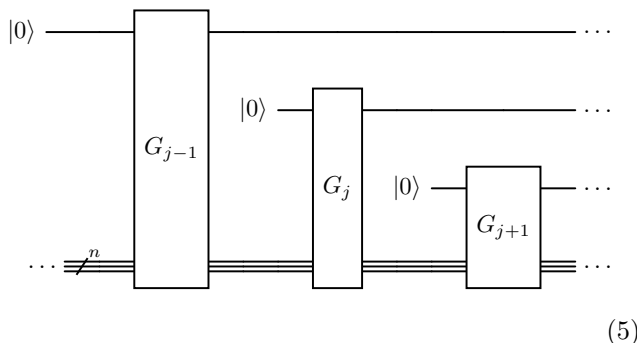


The first operation is a QROM [16] that loads the digitized angles (with b decimals) of the two rotations, θ and ϕ , on two auxiliary qubit registers. As detailed in Sec. III A, these rotations are then performed via phase kickback when arithmetically adding the loaded angles with the phase gradient register $|\nabla_Z\rangle$.

Such phase gradient decompositions are particularly well-suited for a dense arrangement of multiplexed rotation gates. This fact is used in [21], where the authors use a unitary synthesis skeleton based on QR decomposition, taken from optical interferometry [34, 35]. The resulting circuit is a series of phase gradient blocks that realize two consecutive multiplexed phase shift gates, interleaved with incrementer and decremter operations

Reference	R_Y/R_Z count	CNOT count
QR [3] '03	$\lesssim 25 \cdot 4^n$	$\approx 8.7 \cdot 4^n$
CSD [4, 5] '99	$\frac{3}{2} \cdot 4^n - \frac{1}{2} \cdot 2^n$	$\frac{n}{2} \cdot 4^n - \frac{1}{2} \cdot 2^n$
QSD [6] '15	$\frac{3}{2} \cdot 4^n - \frac{3}{2} \cdot 2^n$	$\frac{3}{4} \cdot 4^n - \frac{3}{2} \cdot 2^n$
QSD [31] '25	$\frac{21}{16} \cdot 4^n - \frac{3}{2} \cdot 2^n$	$\frac{9}{16} \cdot 4^n - \frac{3}{2} \cdot 2^n$
QSD [8] '24	$\frac{5}{4} \cdot 4^n - \frac{3}{2} \cdot 2^n + 1$	$\frac{22}{48} \cdot 4^n - \frac{3}{2} \cdot 2^n + \frac{5}{3}$
CSD [18] '04	$4^n - 1$	$4^n - 2 \cdot 2^n$
CSD [19] '04	$4^n - 1$	$\frac{1}{2} \cdot 4^n - \frac{1}{2} \cdot 2^n - 1$
♣-decomp	$4^n - 1$	$\frac{1}{2} \cdot 4^n - \frac{3}{4} \cdot 2^n - 1$
SDM	$4^n - 1$	$\frac{1}{2} \cdot 4^n - \frac{3}{8}(n+2) \cdot 2^n + n - 1$
BWC [32] '25	$4^n - 1$	$\lceil \frac{1}{4} \cdot 4^n - \frac{3n-1}{4} \rceil$
Optimum	$4^n - 1$	$\lceil \frac{1}{4} \cdot 4^n - \frac{3n-1}{4} \rceil$

TABLE I: Known auxiliary-free unitary synthesis techniques into the $\{\text{Clifford} + \text{Rot}\}$ gate set $\{R_Y, R_Z, \text{CNOT}\}$, as well as the contributions of this paper: the flag decomposition (**♣-decomp**), best suited for phase gradient decompositions, and selective de-multiplexing (SDM), which achieves parameter-optimality and CNOT counts close to those in [8]. Based on [8, Tab. 1]. The rows are sorted by decreasing R_Y/R_Z count and then by decreasing CNOT count (for $n > 3$), with lowest achieved counts marked in green. We refer to the Block-ZXZ decomposition [8] as quantum Shannon decomposition (QSD) [1] as they only differ by a choice of subalgebra [9], and all considerations can be transferred between them, leading to the same gate counts. For brevity, we leave out gate counts for Khaneja-Glaser decompositions derived in [7, 31]. Although we consider the full unitary group $U(2^n)$ with 4^n degrees of freedom (including a global phase), the optimal number of R_Y/R_Z is $4^n - 1$. The lower bound for the CNOT gates in the last row [33] is attained by the brick wall circuits (BWC) in [32]. However, this comes at a significant classical computational cost, practically restricting the method to few qubits and hence rendering it unsuitable for MPS preparation.



The horizontal connections in Eq. (4) are the so-called *virtual bonds*. They have a direct correspondence to the

n auxiliary qubits in Eq. (5), which are shared between all the unitaries G_j . The thin vertical lines in Eq. (4) are the so-called physical bonds of dimension $d = 2$ for qubits. The fixed input state $|0\rangle$ in Eq. (5) can be interpreted as a second physical bond that is trivially of dimension 1.

We can use our new unitary synthesis techniques for the G_j unitaries with $4^{n+1} = 4\chi^2$ real parameters each. Due to the specific structure of MPS circuits, we can perform additional optimizations. These manifest in two crucial reductions:

- We use the fixed input state $|0\rangle$ to simplify the circuit structure by removing multiplexer nodes and R_Z rotations, effectively removing χ^2 parameters. This reduction stems from the fact that the tensors A^{σ_j} define isometries with $3\chi^2$ parameters.
- We can merge a unitary with χ^2 parameters on the shared auxiliary n -qubit register from one isometry into its neighbor. This corresponds to the so-called gauge degree of freedom of MPS; see Sec. V and [36, Sec. 4.1.3, iv)].

Overall, this leaves $2\chi^2$ as the optimal number of parameters for each of the G_j in the MPS, which we achieve with our parameter-optimal circuits indicated in Fig. 1 and discussed in detail in Sec. V. The structural improvements of our unitary synthesis circuits and the parameter-optimality with respect to the MPS manifold lead to improved resources compared to the current state of the art in [21]. Further reductions due to boundary effects that have not been previously discussed are provided in App. E2.

III. FLAG DECOMPOSITION

In this section we will derive the so-called *flag decomposition* of a unitary V into a diagonal unitary Δ and a *flag circuit* **♣**. It serves as an essential building block for all the (recursive) parameter-optimal decompositions illustrated in Fig. 1. Further, it improves upon the state of the art in terms of Toffoli counts when utilizing a phase gradient decomposition. We note that the circuit resulting from the flag decomposition derived in this section is equivalent to the circuit obtained from a recursive CSD by Bergholm et al. [19], which we discuss in detail in App. C.

We will show in the following that any unitary $V \in U(2^n)$ with 4^n degrees of freedom can be factorized into a “flag circuit” with $4^n - 2^n$ degrees of freedom and a diagonal matrix with 2^n degrees of freedom:

$$V_{4^n} = \text{♣}_{4^n-2^n} \Delta_{2^n} \quad (6)$$

The component before the diagonal lives in a so-called complete flag manifold⁶

$$\mathbb{F}_{4^n-2^n} \in U(2^n)/\mathbb{T}^{2^n}, \quad (7)$$

where \mathbb{T} refers to the maximal torus, i.e., the maximal Abelian subgroup of diagonal matrices. Each element of the manifold thus is an equivalence class, rather than a specific unitary matrix. A representative of the class can be chosen by fixing one phase per row. For example, we could force the flag unitary to have a real diagonal. Instead, we will fix the representative through the *decomposition* of the flag circuit itself, building on the notion of unitary synthesis “up to a diagonal”. Note, that this makes the representative depend on the particular decomposition that is chosen, leading to a dependency on the target gate set. Alternatively, we can view it as the manifold generated as $\exp(\mathfrak{h})$, where \mathfrak{h} is spanned by the *hollow* matrices with no diagonal entries⁷.

Note that throughout this work, we will consider the unitary group $U(2^n)$ as the total group, including a global phase. This simplifies the presented recursive constructions, as it allows us to attach multiplexing nodes without having to manually track “global” phases that become local phases in the process. Removing the genuinely global phase at the end of the synthesis is a simple task, reducing the parameter count (but not the number of rotation gates) by one.

The simplest flag decomposition for a single qubit comes in the form of the Euler decomposition,

$$\text{---} \boxed{V} \text{---} = \text{---} \boxed{R_Z \ R_Y} \boxed{R_Z \ e^{i\phi}} \text{---} \quad (8)$$

where we interpret the first two gates as the flag circuit with $4^1 - 2^1 = 2$ parameters, and the latter two form a diagonal unitary with the remaining 2 parameters.

For two qubits, we obtain a flag decomposition by modifying Thm. 14 in [1]:

$$\text{---} \boxed{V} \text{---} = \text{---} \boxed{R_Z \ R_Y \ R_Z \ R_Y \ R_Z \ R_Y \ R_Z \ R_Y} \boxed{R_Z \ R_Y \ R_Z \ R_Y \ R_Z \ R_Y \ R_Z \ R_Y \ \Delta} \text{---} \quad (9)$$

⁶ We shall refer to it as just the flag manifold for brevity.

⁷ These hollow matrices form the root spaces of $\mathfrak{u}(2^n)$, so we have the root-space decomposition $\mathfrak{u}(2^n) = \mathfrak{t} \oplus \mathfrak{h} = \mathfrak{t} \oplus \bigoplus_{\alpha} g_{\alpha}$, where \mathfrak{t} is the Lie algebra of the maximal torus \mathbb{T} .

Compared to [1, Thm. 14], we extracted the diagonal to the right end of the circuit, and applied Euler decompositions to all $SU(2)$ gates to reduce the parameter count and distribute the remaining gates into a more regular structure. We note also that the flag circuit here contains six smaller single-qubit flag circuits.

Having seen the one- and two-qubit examples, we now generalize the flag decomposition to arbitrary qubit counts. This decomposition is going to be recursively repeated until one of the two base cases, with one or two qubits, is reached. In the following derivation, we are going to extensively use multiplexers, so recall the following definition for two square matrices $M_0, M_1 \in U(2^{n-1})$, multiplexed on a single qubit:

$$\text{---} \boxed{M_j} \text{---} = \text{---} \boxed{M_0} \boxed{M_1} \text{---} = \begin{pmatrix} M_0 & 0 \\ 0 & M_1 \end{pmatrix}.$$

To derive the general flag decomposition, suppose we are given a unitary matrix $V \in U(2^n)$. First, we perform a cosine-sine decomposition (CSD), which can conveniently be expressed as

$$\text{---} \boxed{V} \text{---} = \text{---} \boxed{K_{1j}} \boxed{K_{0j}} \boxed{R_Y(\theta_Y)} \text{---} \quad (10)$$

Here, operators attached by a single-qubit multiplexer get an index $j \in \{0, 1\}$, for the respective control value. Numerically, the CSD functionality to compute the angles θ_Y for R_Y and the four matrices K_{ij} is readily available in standard linear algebra packages, such as LAPACK [37] or SciPy [28]. For our purposes, `scipy.linalg.cossin` with the option `separate=True` does exactly what we need.

Next, we perform a flag decomposition on each of the two matrices K_{10} and K_{11} , which yields

$$\text{---} \boxed{K_{1j}} \text{---} = \text{---} \boxed{K_{1j}} \boxed{\Delta_{1j}} \text{---} \quad (11)$$

This is where recursion comes into play, as we are performing an $(n-1)$ -qubit flag decomposition inside the n -qubit flag decomposition. We can then use the multiplexer extension property (MEP) [1, Sec. 3.2] that allows us to simply attach multiplexers to circuit identities, which yields

$$(12)$$

We then split a diagonal operator Δ' on the lower n qubits off the multiplexed diagonal [1, 38]:

$$(13)$$

The new diagonal and the $R_Z(\theta) = \exp(-i\frac{\theta}{2}Z)$ rotation angles are given by

$$\Delta' = \sqrt{\Delta_{10}\Delta_{11}} = \exp\left(\frac{i}{2}(\arg(\Delta_{10}) + \arg(\Delta_{11}))\right), \quad (14)$$

$$\theta_Z = \arg(\Delta_{11}\Delta_{10}^*) = \arg(\Delta_{11}) - \arg(\Delta_{10}). \quad (15)$$

We then insert all this back into Eq. (10), commute Δ' through the controls of the multiplexed R_Y rotation, and merge it into the right multiplexer. This yields

$$(16)$$

Note that the multiplexed R_Z and R_Y gates together already constitute a multiplexed single-qubit flag circuit (see Eq. (18) below).

In a last decomposition step, we apply Eq. (12) to $K_{0j} \cdot \Delta'^8$ to obtain Δ_{0j} and $\sqrt{0j}$. This time, we leave the multiplexed diagonal intact. For that, note that a multiplexed diagonal is equivalent to a diagonal, i.e.

$$(16)$$

where the larger diagonal matrix is simply a concatenation of the two smaller diagonals,

$$\Delta = \Delta_{00} \oplus \Delta_{01}. \quad (17)$$

⁸ We will not make a notational difference between diagonal matrices and their diagonal, and standard matrix multiplication is implied throughout.

This then leaves us with the recursive flag decomposition:

$$(18)$$

Note that everything before the diagonal operator constitutes the flag sub-circuit of the decomposition.

Repeating the previous steps on more qubits explicitly, we see the following regular Gray code structure:

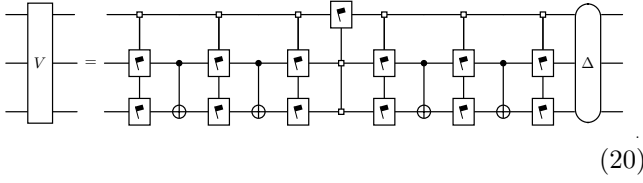
$$(19)$$

The flag sub-circuits have the same Gray code structure. The recursion is continued until the base case of either $n_b = 1$ (Eq. (8)) or $n_b = 2$ (Eq. (9)) qubits is reached.

Hence, for $n = 3$ qubits, we simply obtain the circuit in Eq. (19) with a single qubit in the bottom register for the base case $n_b = 1$:

$$(19)$$

For $n_b = 2$, we can utilize Eq. (9), which leads to

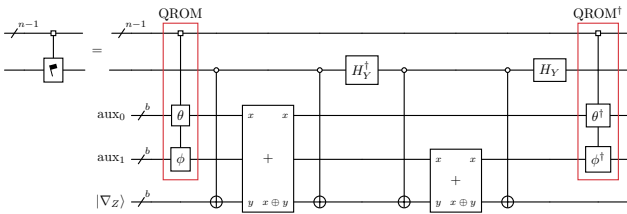


The two base cases lead to different control structures. Depending on how we choose to further decompose the multiplexers, either case can have advantages. The regular structure for the base case $n_b = 1$ is used in the phase gradient decomposition (see Sec. III A) and reproduces the recursive CSD (see App. C). The base case $n_b = 2$ has fewer CNOT gates in the {Clifford + Rot} decomposition, improving upon the recursive CSD, and we detail its decomposition to this gate set in Apps. C 2 and D 2. This decomposition will be superseded by SDM in Sec. IV due to the improved CNOT counts. In SDM, we will employ the $n_b = 2$ recursive flag decomposition as a subroutine; see also App. D for details on this analysis.

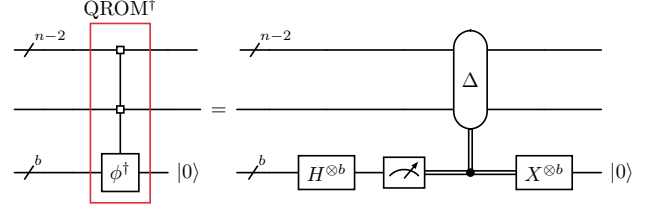
The recursive algorithm with both base cases is summarized in Alg. 1 in App. A 1, including the optional decomposition of multiplexed single-qubit flags into {Clifford+Rot} gates, and implemented as `flagsynth.mux_multi_qubit_decomp` in [30].

A. Phase gradient decomposition

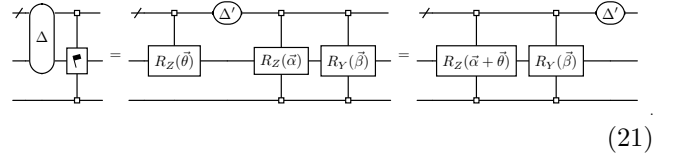
For the phase gradient decomposition, we use Eq. (19) with the base case $n_b = 1$, resulting in $2^n - 1$ multiplexed single-qubit flag operators followed by a diagonal unitary. We provide an overview of the complete decomposition pipeline in Fig. 2. The phase gradient decomposition of the multiplexed single-qubit flag yields the following circuit with additional auxiliary qubit registers onto which the angles are loaded, as well as another register carrying a phase gradient state $|\nabla_Z\rangle$:



Here, b is the number of digits we use to encode the angles in their binary representation. More details and a full derivation can be found in App. B 4 and [39]. The second QROM, which uncomputes the loaded angles, can be performed with measurements and a classically controlled diagonal operator,



This diagonal operator can be merged into the subsequent multiplexed flag of the circuit skeleton in Eq. (19), such that it does not invoke any additional cost:



Here, $\vec{\alpha}$ and $\vec{\beta}$ represent the rotation angles of the multiplexer we aim to merge the diagonal into. The vector $\vec{\theta}$ is given by Eq. (15) and Eq. (17)⁹.

When uncomputing the QROM of the next multiplexer, a new classically controlled diagonal is generated. The previously computed diagonal Δ' is then merged into the new diagonal, allowing the process to be repeated until the last multiplexer is reached. The final classically controlled diagonal operation can be merged with the very final diagonal gate on the right in Fig. 2.

After this optimization, the Toffoli cost for each of the $2^n - 1$ multiplexers is given by

$$C_{\text{Tof}}^{\text{mux-}\Lambda} = \frac{2^n}{2\Lambda} + 2\Lambda b - 5, \quad (22)$$

where b is the number of bits used to represent the rotations and Λ ¹⁰ is a tuneable parameter that represents the number of rows defined in the QROM structure. A detailed derivation of this cost can be found in App. B 4.

The final diagonal Δ can also be decomposed using phase gradient states and leads to the cost

$$C_{\text{Tof}}^{\Delta} = \frac{2^n}{2\Lambda} + 2\Lambda b + \frac{2^n}{\Lambda'} + \Lambda' - 5. \quad (23)$$

The two different values Λ and Λ' are due to the usage of two separate QROMs: one that stores bitstrings of size b with 2Λ rows, and a second one that stores bitstrings

⁹ Note that the angles in $\vec{\theta}$ need to be extended to match the dimension of $\vec{\alpha}$, which is additionally multiplexed by the lower qubit register. This can be achieved by $\theta \otimes (1, 1)$.

¹⁰ Given k available auxiliary qubits in the circuit, we can estimate Λ as the closest power of two to $\min\left(\left\lceil \sqrt{2^m/b} \right\rceil, k/b\right)$, where m is the number of QROM control qubits.

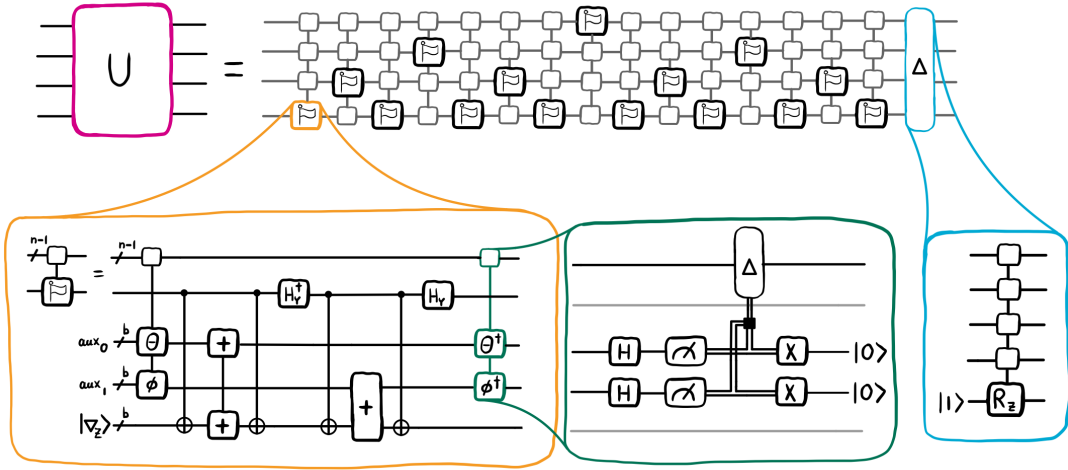


FIG. 2: Phase gradient decomposition of our unitary synthesis circuit. The unitary is first broken down into $(n - 1)$ -multiplexed single-qubit flags and a trailing diagonal via a recursive flag decomposition (top circuit). Each multiplexed flag can be implemented via loading of the flag angles θ and ϕ , adds onto a resource phase gradient state $|\nabla_Z\rangle$ that are control-flipped by the flag target into subtractors, and angle unloading (orange, bottom left). The latter is implemented via measurement in the X basis and a corrective diagonal, which depends on the measurement outcomes and can be merged into subsequent flags (dark green, bottom mid). The terminal diagonal is implemented as a multiplexed R_Z gate on a fixed-state qubit (blue, bottom right); see App. B 5 for details.

of size 1 with Λ' rows. A detailed description is provided in App. B 5. Therefore, the total cost of the unitary synthesis technique is:

$$C_{\text{Tof}}^{\square\text{-decomp}} = (2^n - 1) C_{\text{Tof}}^{\text{mux-}\square} \text{ (flag multiplexers)} \\ + C_{\text{Tof}}^{\Delta} \text{ (final diagonal)}. \quad (24)$$

This is an improvement over the decomposition in [21] with cost¹¹:

$$C_{\text{Tof}}^{[21]} = 2^n C_{\text{Tof}}^{\text{mux-}\square} \text{ (phase multiplexers)} \\ + C_{\text{Tof}}^{\Delta} \text{ (final diagonal)} \\ + C_{\text{Tof}}^{\pm 1} \text{ (incrementers/decrementers)}.$$

Here, the additional cost of the incrementers and decrementers is given by $C_{\text{Tof}}^{\pm 1} = (2^n - 1)(n - 2)$, since the cost of an adder with a classical input is $n - 2$ [17]. The cost for multiplexed phases is the same as for the multiplexed single-qubit flag circuit. These savings are due to the structure of the flag decomposition circuit in Fig. 2. The parameters are distributed in an optimal fashion among the $2^n - 1$ multiplexers. On the other hand, the Gray code structure removes the necessity for incrementers and decrementers, and still allows us to merge the classically controlled diagonals from the QROM uncomputations

with measurements. Compared to [21], we overall reduce the Toffoli gate count by

$$C_{\text{Tof}}^{\text{mux-}\square} + C_{\text{Tof}}^{\pm 1} = \left(\frac{2^n}{2\Lambda} + 2\Lambda b - 5 \right) + (n - 2)(2^n - 1). \quad (25)$$

IV. SELECTIVE DE-MULTIPLEXING

As we have seen in the previous section, the flag decomposition is well-suited for phase gradient decompositions. In the context of {Clifford + Rot} decompositions, it is already parameter-optimal and provides a reasonable CNOT count of $\frac{1}{2}4^n - \frac{3}{4}2^n - 1$, as reported in Tab. I. We can further improve this to a CNOT count of $\frac{1}{2}4^n - \frac{3}{8}(n + 2)2^n + n - 1$, matching the best known CNOT count reported in Krol et al. [8] for $n \in \{3, 4\}$. This is achieved by what we call *selective de-multiplexing (SDM)*, illustrated in Fig. 3. The procedure builds on the quantum Shannon decomposition, but in order to remain parameter-optimal after the first recursion step, we introduce selective de-multiplexing for flag circuits in Sec. IV B. Thus, we are selective both across the depth of the recursion and across the circuit length about which multiplexers to de-multiplex.

We start out just like the original QSD [1], performing a CSD followed by de-multiplexing in the first recursive step (a type-AIII + type-A recursive Cartan decomposition [9]). However, we then modify the circuit using the flag decomposition from Sec. III to achieve and maintain parameter optimality; see Sec. IV A. This results in a richer recursion structure and forces us to decompose

¹¹ See Eq. (2) for the corresponding circuit structure.

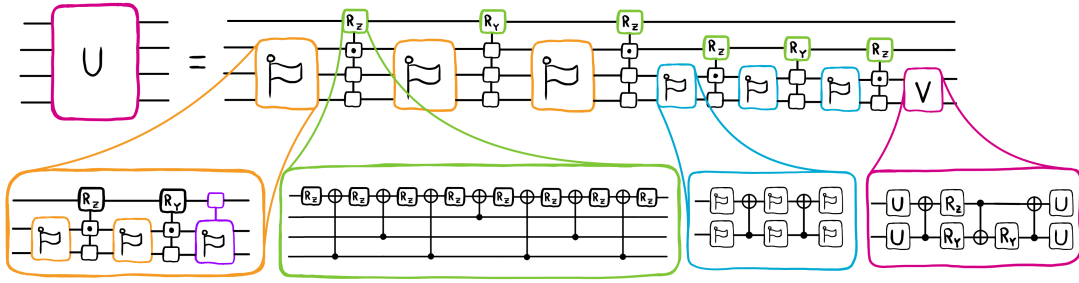


FIG. 3: Selective de-multiplexing (SDM) proposed in this work. A unitary operator is decomposed with a single QSD step in a parameter-optimal fashion (Sec. IV A, top circuit), producing flag circuits, multiplexed rotations, and a smaller unitary. These constituents are decomposed by selectively de-multiplexing the flag circuit (orange, lower left, Sec. IV B), a (symmetrized) Möttönen decomposition (green, lower left mid, Eq. (29)) and a next QSD step using SDM. Ultimately, we use known base case decompositions for two-qubit flags (blue, lower right mid, Eq. (9)) and two-qubit unitaries (magenta, lower right, Eq. (32)). Multiplexed flags (purple) are decomposed with the recursive flag decomposition/CSD from Sec. III (not shown here).

multiple different multi-qubit operators from the second step onwards, which we analyze in App. D. Finally, we selectively de-multiplex flag circuits during the recursion in order to lower the CNOT count; see Sec. IV B. We put all pieces of SDM together in Sec. IV C. As the phase gradient decomposition does not benefit from SDM, we target the {Clifford + Rot} decomposition for the rest of this section.

A. Making a single QSD step parameter-optimal

As in Eq. (10), we first decompose a given unitary from $V \in U(2^n)$ via a CSD:

$$(26)$$

Instead of decomposing the matrices K_{ij} inside the multiplexers, we now de-multiplex these operators,

$$(27)$$

Note that we now omit the first subscript of K and M for better readability. The matrices for this type-A decomposition are computed as follows. We perform an eigenvalue decomposition of $K_0 K_1^\dagger$ as $M_0 D^2 M_0^\dagger$ and set $M_1 = D M_0^\dagger K_1$ [1]. The Z -rotation angles are given by

the phases of the diagonal, $\theta_Z = -2 \arg(D)$. Putting the CSD and the de-multiplexing together, we arrive at

$$(27)$$

where $M_{jk} \in U(2^{n-1})$. Before decomposing these M_{jk} , we perform a small optimization that was introduced in [1] and extended in [8]. For this, we re-assemble M_{10} , M_{01} and the R_Y multiplexer into a multiplexed unitary, where the multiplexing qubit now acts in the Pauli- Y basis, and insert identities in the form of CY^2 :

$$(28)$$

The gates in the center red box can then be merged and de-multiplexed again, while the decomposition of the R_Z multiplexers can be chosen to produce a CY gate to the right or left, such that it cancels with the created gate in each blue box. The result is a symmetrized variant of the Möttönen decomposition, which we mark with a dot in the corresponding multiplexing node:

$$(29)$$

The crucial part of this decomposition is that we save one entangling gate compared to the standard multiplexer decomposition [40, 41]; see App. D 2 for further details. Note that we could instead choose to symmetrize any other two of the three multiplexed rotations.

We continue with a flag decomposition $M_{11} = \Delta_{11} \mathbb{V}_{11}$, commute its diagonal Δ_{11} through the left-most multiplexed rotation (and CY gate), and compute $M'_{10} = M_{10} \Delta_{11} \in U(2^{n-1})$. Consecutively repeating these steps for the other matrices, we arrive at

$$(30)$$

We are left with the unitary $V' = M_{00} \Delta_{01}$, which can be decomposed recursively by applying all steps described in this section again, beginning with the CSD.

What remains are flag circuits, which we could decompose with the strategy from Sec. III. However, there is an alternative inspired by the QSD, which we term *selective de-multiplexing* and detail in the next section. For brevity, we move the discussion about why selective de-multiplexing is preferred over flag circuits in the context of {Clifford + Rot} decompositions to App. D 3.

B. Selective de-multiplexing of a flag circuit

When decomposing a flag circuit recursively with the flag decomposition from Sec. III, we may take a slight detour that is inspired by the de-multiplexing in the QSD above. Namely, after executing the first CSD like in Eq. (26), we may apply the de-multiplexing to the first of the two multiplexed flags only, leading to the following circuit¹²:

$$(31)$$

Here, we already commuted a diagonal through the circuit, and used the trick in Eq. (28) to symmetrize both

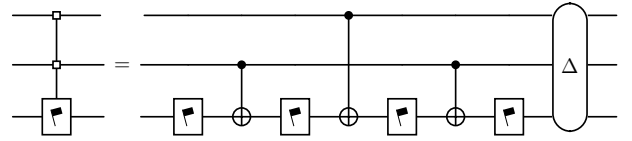
multiplexed rotations, by producing a CY gate between the multiplexed R_Z and \mathbb{V}_{10} as well as a CZ between the multiplexed R_Y and \mathbb{V}_0 . This selective de-multiplexing step maintains parameter optimality¹³, and we will employ it to obtain our cheapest decomposition; see the following section and App. D for details.

C. Assembling the selective de-multiplexing synthesis

We now have collected all pieces to assemble the complete synthesis procedure using SDM. For unitaries, we use a parameter-optimal QSD step with a symmetrized Möttönen decomposition for multiplexed rotations (see Sec. IV A), until we reach the well-known two-qubit base case:

$$(32)$$

Here, the diamond-shaped gate denotes a global phase $e^{i\alpha}$. Non-multiplexed flag circuits are broken down via a CSD and selective de-multiplexing (see Eq. (31)) whereas multiplexed flag circuits are decomposed with pure recursive CSDs. For both multiplexed and non-multiplexed flags, we make use of the decomposition on $n_b = 2$ qubits, shown in Eq. (9), as the base case. Ultimately, multiplexed single-qubit flags are expressed in the elementary gate set with a technique from [19], shown here for $n = 3$ qubits:



We provide a detailed analysis for these optimized decompositions in App. D, illustrate the SDM procedure in Fig. 3 for $n = 4$ qubits, and summarize it in Algs. 2 and 3 in App. A 1.

Regarding the gate counts, we first consider the parameter count to verify parameter-optimality. In Eq. (30), we see three flag sub-circuits with $4^{n-1} - 2^{n-1}$ parameters each, as we have removed $3 \cdot 2^{n-1}$ parameters via diagonal merging. These removed parameters exactly offset the $3 \cdot 2^{n-1}$ parameters contributed by the three multiplexed rotations. Together with the 4^{n-1} parameters from the final V' , we overall have $4 \cdot 4^{n-1} = 4^n$ parameters, which is optimal for an n -qubit unitary.

¹² Note that we may apply the CSD to the flag circuit as we would to any unitary matrix. This causes overparametrization which is fixed subsequently by merging diagonals.

¹³ Again considering the diagonal produced by the CSD step as “mitigable overparametrization”.

Considering the CNOT count associated with a single QSD step, we obtain the relation

$$C_{\text{CNOT}}^{\text{QSD}}(n) = C_{\text{CNOT}}(n-1) + 3(C_{\text{CNOT}}^{\text{flag}}(n-1) + 2^{n-1}) - 2, \quad (33)$$

which is based on Eq. (30) and the technique from Eqs. (28) and (29) to reduce the CNOT cost for two of the multiplexed rotations by one.

In App. D 3, we compute the minimal CNOT cost of a flag circuit to be

$$C_{\text{CNOT}}^{\text{flag}}(n) = \frac{1}{2}4^n - \frac{n+6}{4}2^n + 1, \quad (34)$$

using selective de-multiplexing for non-multiplexed flags and the recursive flag decomposition from Sec. III for multiplexed flags. This is then inserted into the recursion relation above, together with the base case $C_{\text{CNOT}}(2) = 3$ from the standard two-qubit unitary decomposition in Eq. (32) to obtain the final CNOT count of SDM,

$$C_{\text{CNOT}}^{\text{SDM}}(n) = \frac{1}{2}4^n - \frac{3}{8}(n+2)2^n + n - 1. \quad (35)$$

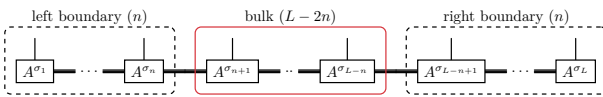
V. MATRIX PRODUCT STATE PREPARATION

Preparing matrix product states (MPS) on a quantum computer is a crucial subroutine for many quantum algorithms. A prominent example is quantum phase estimation, where the overlap of the initial state with the target state is crucial [16, 20, 21]. The improved unitary synthesis techniques introduced in Figs. 2 and 3 translate to improved resources for MPS preparation. An overview of the resulting circuits for both the {Clifford + Rot} and the phase gradient decomposition is provided in Fig. 4.

We consider an MPS with open boundary conditions on L physical sites of local dimension $d = 2$ (for qubits). This state is formally defined in terms of the tensors $\{A^{\sigma_j}\}_{j=1}^L$ as

$$|\psi\rangle = \sum_{\sigma_1 \dots \sigma_L \in \{0,1\}} A^{\sigma_1} \dots A^{\sigma_L} |\sigma_1 \dots \sigma_L\rangle, \quad (36)$$

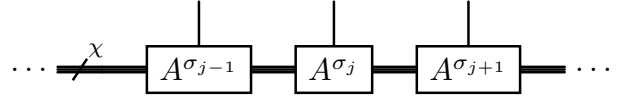
where each of the A^{σ_j} is interpreted as a matrix for the concrete value of $\sigma_j \in \{0,1\}$. The matrix dimensions of A^{σ_j} are slightly different at the left and right boundaries of the MPS. We are going to discuss these boundary effects separately in App. E 2, and here focus on the central *bulk* tensors of the MPS:



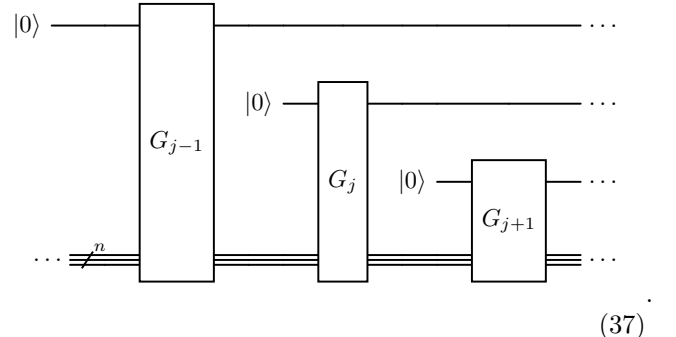
In the bulk, all matrix dimensions (horizontal connections) are truncated to the so-called bond dimension χ . This is a hyper-parameter that determines the degree of

approximation of the MPS. We conveniently choose it to be 2^n , such that we can map it to an n -qubit register. This is highly desired for MPS preparation because there are significant overparametrizations otherwise. This also determines the boundary region to span exactly n tensors on either side of the bulk, which itself comprises $L - 2n$ tensors.

We assume the tensors to define isometries, implying $\sum_{\sigma_j \in \{0,1\}} (A^{\sigma_j})^\dagger A^{\sigma_j} = \mathbf{1}$ and that they map from n to $n-1$ qubits. This can always be achieved by transforming the tensors into the so-called left-canonical form; see [42]. To prepare an MPS on a quantum computer, we translate the isometry tensors



into unitary matrices G_j via unitary completion. The resulting circuit then has the following structure:



In general, an isometry from n to $n+1$ qubits has $3 \cdot 4^n$ degrees of freedom, as it lives on a so-called Stiefel manifold¹⁴. In particular for our case with $\chi = 2^n$, we need to reduce the degrees of freedom of the unitary G_j from $4\chi^2$ to $3\chi^2$. As we will see, this is achieved by removing multiplexer nodes and R_Z gates due to the fixed $|0\rangle$ input.

Further, we will be able to remove another χ^2 degrees of freedom by merging unitaries on the shared auxiliary n -qubit register in Eq. (37) between the isometries. This corresponds to the so-called gauge degree of freedom of MPS. It is due to the ambiguity of the A^{σ_j} isometries, as we can always insert arbitrary unitary matrices W_j and W_j^\dagger on the horizontal connections (the so-called virtual

¹⁴ The Stiefel manifold dimension is $2 \cdot 2^n \cdot 2^m - (2^m)^2$, for an isometry from m to n qubits with $m \leq n$.

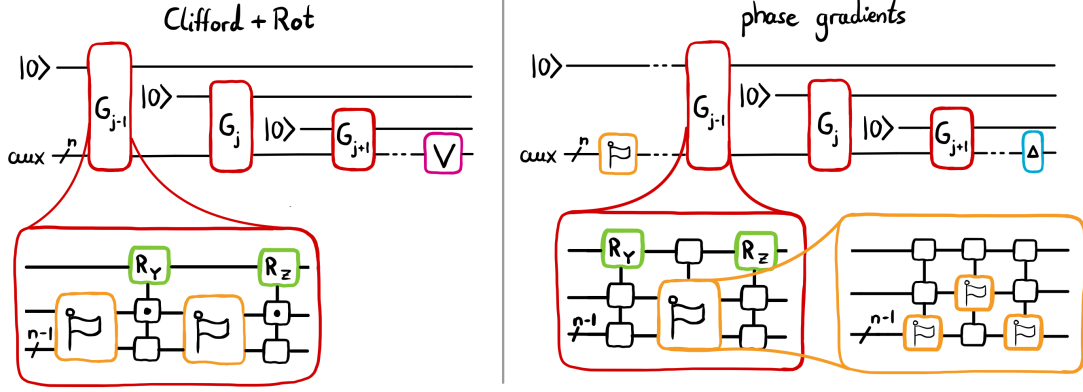
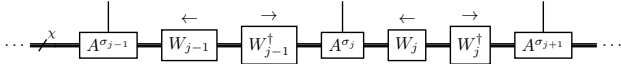


FIG. 4: Decomposition of matrix product state (MPS) preparation using our unitary synthesis results and further optimizations. For each tensor of the MPS (red), we obtain a multiplexed R_Y gate and a subcircuit representing a reduced multiplexed unitary operator. The exact structure of this subcircuit depends on the target gate set, i.e., on whether we compile for the {Clifford + Rot} decomposition (left) or the phase gradient decomposition (right). The resulting (multiplexed) flags and rotations, as well as the trailing diagonal gate Δ are then decomposed with the respective techniques from Figs. 2 and 3. Note that for the phase gradient decomposition, the unitary degrees of freedom on the auxiliary register are split into a flag circuit and a diagonal on either side.

bonds):



By multiplying the unitary matrices in the direction indicated by the arrows, we can arrive at altered isometries A^{σ_j} that define the same state. This ambiguity reduces the free parameters of the isometries by another χ^2 . For more details on the gauge degree of freedom we refer to Sec. 4.1.3, iv) in [36].

In summary, we attain the optimal number of parameters,

$$2\chi^2 \quad (38)$$

for each unitary G_j with the following steps:

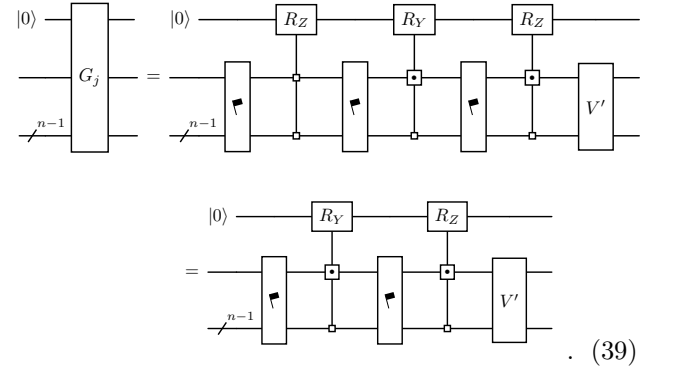
1. Parameter-optimal unitary synthesis ($4\chi^2$): Synthesis of G_j using the circuits in Fig. 1.
2. Isometry condition ($3\chi^2$): Use the fixed input state $|0\rangle$ on the top qubit to remove multiplexer nodes and R_Z rotations.
3. Gauge freedom ($2\chi^2$): Merge a unitary on the shared auxiliary n -qubit register between isometries.

We will go through these steps for each of the considered decomposition methods in the following two subsections.

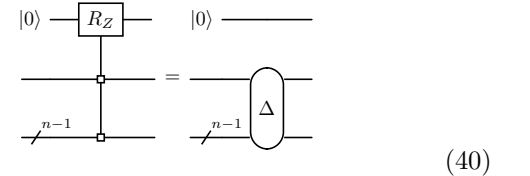
A. {Clifford + Rot} decomposition

For {Clifford + Rot} decomposition, we substitute SDM from Fig. 3 for the unitaries G_j . We apply the

symmetrization trick in Eqs. (28) and (29) to the second and third multiplexers instead:

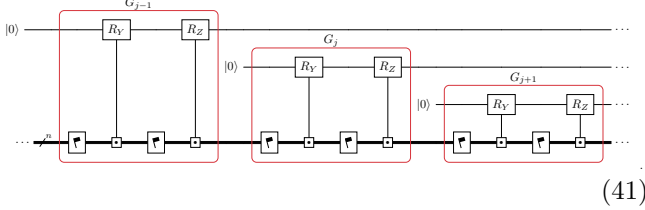


The reductions left of the R_Y multiplexer compared to Eq. (30) are due to the fixed initial state on the first qubit. The multiplexed R_Z is reduced to a diagonal on the lower n qubits,



and can be merged together with the two flags into a new n -qubit unitary. This new unitary can then be flag-decomposed and its diagonal merged to the right again. Because a flag circuit has $4^n - 2^n = \chi^2 - \chi$ parameters, this circuit matches the expected $2(\chi^2 - \chi) + 2\chi + \chi^2 = 3\chi^2$ parameters for a single isometry.

Further, we can merge the unitary V' into the consequent isometry. This corresponds to the gauge freedom of the MPS, which subtracts another χ^2 parameters, overall matching the optimal parameter count in Eq. (38). Thus, we arrive at the following circuit structure¹⁵:



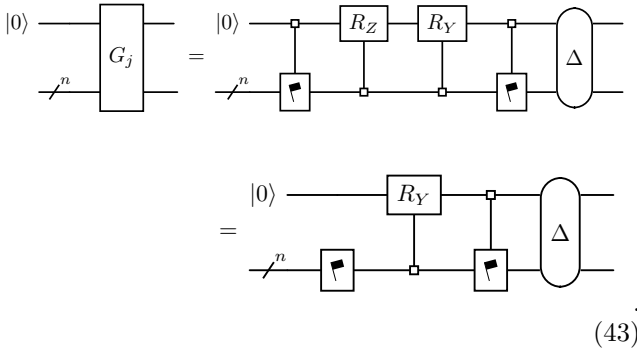
Note that this synthesis procedure requires a causal ordering from left to right. We first synthesize G_{j-1} like in Eq. (39), then merge its V' into G_j , and then continue to synthesize it. Not shown here are additional savings at the boundary; see App. E 2.

Since we target the {Clifford + Rot} decomposition in this section, let us determine the CNOT cost. The cost for each constituent of the G_j circuit is provided in Tab. II. In particular, each symmetrized multiplexed single-qubit rotation costs $2^n - 1$ CNOTs, and each n -qubit flag circuit costs another $\frac{1}{2}4^n - \frac{n+12}{8}2^n + 1$. In total we obtain a CNOT cost of

$$C_{\text{CNOT}}^{G_j} = 4^n - \frac{n+4}{4}2^n. \quad (42)$$

B. Phase gradient decomposition

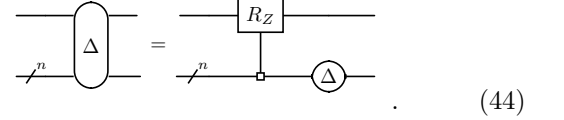
In this section, we will use the unitary synthesis circuit from Fig. 2 for a phase gradient decomposition in the MPS preparation circuit Eq. (37). We again start by removing χ^2 parameters due to the fixed initial state, corresponding to the isometry condition of A^{σ_j} (and, hence, G_j):



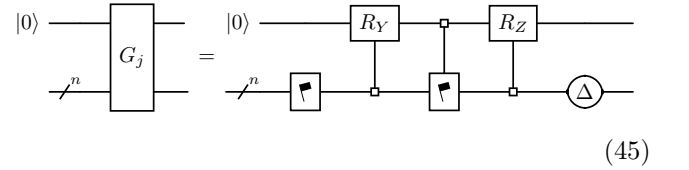
¹⁵ The dotted multiplexer on n qubits here is to be interpreted like above, with one dotted multiplexer node and $(n-1)$ usual multiplexer nodes.

The remaining n -qubit flag left of the R_Y multiplexer is the one that triggers on 0 on the first qubit. Like in Eq. (40), the R_Z multiplexer with $|0\rangle$ as its input on the target qubit yields a diagonal on the multiplexing qubits, which can be merged to the right. We confirm that we now have $(4^n - 2^n) + 2^n + 2 \cdot (4^n - 2^n) + 2^{n+1} = 3 \cdot 4^n = 3\chi^2$ parameters.

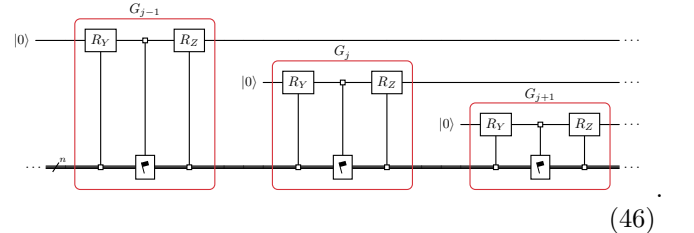
We now remove another χ^2 parameters by merging unitaries on the auxiliary n -qubit register (note that this corresponds to removing the gauge degree of freedom of the MPS). To achieve this, we first split the diagonal gate (see Eqs. (13) and (16)),



This then leaves us with



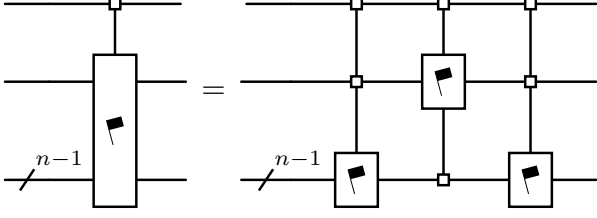
for the individual isometries. The diagonal on the auxiliary n -qubit register can be merged to the right, and the n -qubit flag to the left in the MPS preparation circuit Eq. (37). We note that because we merge to both left and right, the causal ordering in which the decompositions are performed for each G_j is non-trivial and detailed for the full synthesis process in App. E 1. Overall, we obtain the following circuit structure:



Compared to Eq. (41), we have one multiplexed flag instead of two individual n -qubit flags, which is better suited for a phase gradient decomposition. Overall, we achieve the desired optimal $2\chi^2$ parameters from Eq. (38).

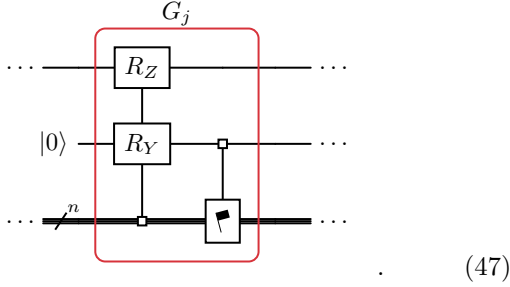
Let us now determine the Toffoli cost for each isometry G_j . The multiplexed flag contributes $2^n - 1$ multiplexed single-qubit flags,

VI. CONCLUSION



Each of the multiplexers is now implemented using the phase gradient decomposition from Sec. III A. The classically controlled diagonal gates that arise in the uncomputation of the QROM for each multiplexer can again be merged and pushed through all layers as done in Eq. (21), then merged with the final multiplexed R_Z rotation.

Further, we can combine the final multiplexed R_Z with the subsequent multiplexed R_Y from the next isometry, creating the following circuit building block:



This combined R_Z and R_Y multiplexer on two separate qubits has the same cost as a multiplexed single-qubit flag. So we overall have $(2^n - 1) + 1 = 2^n$ multiplexers. Each of them contribute the Toffoli cost $\frac{2^{n+1}}{2\Lambda} + 2\Lambda b - 5$ of a single qubit flag circuit, as detailed in App. B 4.

The total cost for an isometry G_j is then given by

$$C_{\text{Tof}}^{G_j} = 2^n \left(\frac{2^{n+1}}{2\Lambda} + 2\Lambda b - 5 \right) \text{ (flag multiplexers).}$$

When we compare this with the Toffoli cost provided in [21],

$$\begin{aligned} C_{\text{Tof}}^{[21]} &= 2^n \left(\frac{2^{n+1}}{2\Lambda} + 2\Lambda b - 5 \right) \text{ (phase multiplexers)} \\ &+ \frac{2^{n+1}}{2\Lambda} + 2\Lambda b + \frac{2^{n+1}}{\Lambda'} + \Lambda' - 5 \text{ (final diagonal)} \\ &+ ((n+1) - 3)(2^{n+1}/2 - 1) \text{ (incrementers)} \\ &+ \frac{2^{n+1}}{2\Lambda} + \Lambda b - 2 \text{ (controlled qubit rotation),} \end{aligned}$$

we see that we save the final diagonal, the multiplexed n -qubit rotation, as well as not requiring incrementers and decrementers due to the improved synthesis method. This is achieved by utilizing flag decompositions to ensure parameter-optimality with respect to the MPS manifold.

In this work, we introduce the *flag decomposition* as a central tool for synthesis of unitaries and isometries. It enables us to produce parameter-optimal quantum circuits for generic unitaries and matrix product state (MPS) preparation that improve upon the state of the art, both when compiling down to the {Clifford+Rot} gate set and when using the phase gradient decomposition.

We find that the recursive flag decomposition yields the same circuit as a synthesis technique from 2004 [19], that, to our knowledge, has been mostly underappreciated, if not forgotten. Striving for a reduction in CNOT counts, the literature dismissed it in favour of the quantum Shannon decomposition (QSD, 2004 [33]) and, in a recent upgrade, the Block-ZXZ decomposition (2024, [8]). While they lowered the CNOT count, these techniques introduced a significant overparametrization, which presents an unfavourable tradeoff for fault-tolerant quantum computation.

For {Clifford + Rot} decompositions, we further improve upon the recursive flag decomposition. For this, we draw inspiration from a key innovation of the QSD, called de-multiplexing. While it leads to overparametrization when applied greedily, we are able to avoid this problem after a careful cost analysis, by applying it *selectively*, across both the recursion levels and the circuit depth. This leads us to *selective de-multiplexing* (SDM), our second parameter-optimal synthesis method, with improved CNOT counts over the recursive flag decomposition for {Clifford + Rot} decompositions.

We then use our new synthesis techniques to compile MPS preparation circuits, a crucial subroutine for a number of promising quantum algorithms, in particular in the context of quantum chemistry and material design applications. Our techniques prove well-suited for the adjustment to the isometry synthesis needed for this task, and the flag decomposition allows us to further optimize the resulting circuits. In addition, we exploit the mathematical framework of recursive Cartan decompositions to adjust our synthesis to the conditions at the boundary of the MPS, maintaining parameter-optimality where existing simplifications cannot. Our detailed cost analysis shows that we again improve over the best known methods both for the {Clifford + Rot} decomposition and the phase gradient decomposition.

Once recognized, flag decompositions—and the resulting “flag circuits”—can be found across the unitary synthesis literature. This underlines their usefulness for both unifying and advancing the field, and we believe that developing a systematic (Lie) group-based framework and computational toolbox will continue to prove fruitful for quantum compilation of parametric gate families.

Future research questions on unitary synthesis span a wide range, from mathematical questions about whether lower bounds on the CNOT count and circuit depth can be achieved, to practical analyses of approximate compi-

lation and hybrid decompositions between the {Clifford + Rot} gate set and phase gradient rotations motivated by space constraints. Regarding the minimal achievable CNOT count, recent progress on small-scale synthesis suggests that saturating both the CNOT and the rotation

lower bounds simultaneously is possible, but an efficient linear algebra synthesis technique remains elusive [32]. A systematic extension of the group-based perspective to more specific circuit structures would be another interesting direction to consider, bridging unitary synthesis to other fields in quantum compilation.

-
- [1] V.V. Shende, S.S. Bullock, and I.L. Markov. “Synthesis of quantum-logic circuits”. *IEEE Transactions on Computer-Aided Design of Integrated Circuits and Systems* **25**, 1000–1010 (2006). [arXiv:quant-ph/0406176](#).
- [2] Navin Khaneja and Steffen J Glaser. “Cartan decomposition of $SU(2^n)$ and control of spin systems”. *Chem. Phys.* **267**, 11–23 (2001). [arXiv:quant-ph/0010100](#).
- [3] Juha J Vartiainen, Mikko Möttönen, and Martti M Salomaa. “Efficient decomposition of quantum gates”. *Phys. Rev. Lett.* **92**, 177902 (2004). [arXiv:quant-ph/0312218](#).
- [4] Robert R. Tucci. “A rudimentary quantum compiler(2cnd ed.)” (1999). [arXiv:quant-ph/9902062](#).
- [5] Anna M. Krol, Aritra Sarkar, Imran Ashraf, Zaid Al-Ars, and Koen Bertels. “Efficient decomposition of unitary matrices in quantum circuit compilers”. *Applied Sciences* **12**, 759 (2022). [arXiv:2101.02993](#).
- [6] A. De Vos and S. De Baerdemacker. “Block-ZXZ synthesis of an arbitrary quantum circuit”. *Phys. Rev. A* **94**, 052317 (2016). [arXiv:1512.07240](#).
- [7] Maximilian Balthasar Mansky, Santiago Londoño Castillo, Victor Ramos Puigvert, and Claudia Linnhoff-Popien. “Near-optimal quantum circuit construction via Cartan decomposition”. *Physical Review A* **108** (2023). [arXiv:2212.12934](#).
- [8] Anna M. Krol and Zaid Al-Ars. “Beyond quantum shannon decomposition: Circuit construction for n -qubit gates based on Block-ZXZ decomposition”. *Phys. Rev. Appl.* **22**, 034019 (2024). [arXiv:2403.13692](#).
- [9] David Wierichs, Maxwell West, Roy T. Forestano, M. Cerezo, and Nathan Killoran. “Recursive Cartan decompositions for unitary synthesis” (2025). [arXiv:2503.19014](#).
- [10] Austin G. Fowler, Matteo Mariantoni, John M. Martinis, and Andrew N. Cleland. “Surface codes: Towards practical large-scale quantum computation”. *Physical Review A* **86** (2012). [arXiv:1208.0928](#).
- [11] Daniel Litinski. “A Game of Surface Codes: Large-Scale Quantum Computing with Lattice Surgery”. *Quantum* **3**, 128 (2019). [arXiv:1808.02892](#).
- [12] Christopher M. Dawson and Michael A. Nielsen. “The Solovay-Kitaev algorithm”. *Quantum Info. Comput.* **6**, 81–95 (2006). [arXiv:quant-ph/0505030](#).
- [13] Neil J. Ross and Peter Selinger. “Optimal ancilla-free Clifford+T approximation of Z-rotations”. *Quantum Info. Comput.* **16**, 901–953 (2016). [arXiv:1403.2975](#).
- [14] Alex Bocharov, Martin Roetteler, and Krysta M. Svore. “Efficient synthesis of universal repeat-until-success quantum circuits”. *Phys. Rev. Lett.* **114** (2015). [arXiv:1404.5320](#).
- [15] Vadym Kliuchnikov, Kristin Lauter, Romy Minko, Adam Paetznick, and Christophe Petit. “Shorter quantum circuits via single-qubit gate approximation”. *Quantum* **7**, 1208 (2023). [arXiv:2203.10064](#).
- [16] Guang Hao Low, Vadym Kliuchnikov, and Luke Schaeffer. “Trading T gates for dirty qubits in state preparation and unitary synthesis”. *Quantum* **8**, 1375 (2024). [arXiv:1812.00954](#).
- [17] Craig Gidney. “Halving the cost of quantum addition”. *Quantum* **2**, 74 (2018). [arXiv:1709.06648](#).
- [18] Mikko Möttönen, Juha J. Vartiainen, Ville Bergholm, and Martti M. Salomaa. “Quantum circuits for general multiqubit gates”. *Phys. Rev. Lett.* **93**, 130502 (2004). [arXiv:quant-ph/0404089](#).
- [19] Ville Bergholm, Juha J Vartiainen, Mikko Möttönen, and Martti M Salomaa. “Quantum circuits with uniformly controlled one-qubit gates”. *Phys. Rev. A* **71**, 052330 (2005). [arXiv:quant-ph/0410066](#).
- [20] Stepan Fomichev, Kasra Hejazi, Modjtaba Shokrian Zini, Matthew Kiser, Joana Fraxanet, Pablo Antonio Moreno Casares, Alain Delgado, Joonsuk Huh, Arne-Christian Voigt, Jonathan E. Mueller, and Juan Miguel Arrazola. “Initial state preparation for quantum chemistry on quantum computers”. *PRX Quantum* **5**, 040339 (2024). [arXiv:2310.18410](#).
- [21] Dominic W. Berry, Yu Tong, Tanuj Khattar, Alec White, Tae In Kim, Guang Hao Low, Sergio Boixo, Zhiyan Ding, Lin Lin, Seunghoon Lee, Garnet Kin-Lic Chan, Ryan Babbush, and Nicholas C. Rubin. “Rapid initial-state preparation for the quantum simulation of strongly correlated molecules”. *PRX Quantum* **6**, 020327 (2025). [arXiv:2409.11748](#).
- [22] C. Schön, E. Solano, F. Verstraete, J. I. Cirac, and M. M. Wolf. “Sequential generation of entangled multiqubit states”. *Phys. Rev. Lett.* **95**, 110503 (2005). [arXiv:quant-ph/0501096](#).
- [23] Tsung-Cheng Lu, Leonardo A. Lessa, Isaac H. Kim, and Timothy H. Hsieh. “Measurement as a shortcut to long-range entangled quantum matter”. *PRX Quantum* **3**, 040337 (2022). [arXiv:2206.13527](#).
- [24] Kevin C. Smith, Abid Khan, Bryan K. Clark, S.M. Girvin, and Tzu-Chieh Wei. “Constant-depth preparation of matrix product states with adaptive quantum circuits”. *PRX Quantum* **5**, 030344 (2024).
- [25] David Wierichs. “Constant-depth preparation of matrix product states with dynamic circuits”. https://pennylane.ai/qml/demos/tutorial_constant_depth_mps_prep (2024).
- [26] Zhi-Yuan Wei, Daniel Malz, and J. Ignacio Cirac. “Efficient adiabatic preparation of tensor network states”. *Phys. Rev. Res.* **5**, L022037 (2023). [arXiv:2209.01230](#).
- [27] Daniel Malz, Georgios Styliaris, Zhi-Yuan Wei, and J. Ignacio Cirac. “Preparation of matrix product states with log-depth quantum circuits”. *Phys. Rev. Lett.* **132**, 040404 (2024). [arXiv:2307.01696](#).
- [28] Pauli Virtanen, Ralf Gommers, Travis E Oliphant, Matt Haberland, Tyler Reddy, David Cournapeau, Evgeni

- Burovski, Pearu Peterson, Warren Weckesser, Jonathan Bright, et al. “SciPy 1.0: fundamental algorithms for scientific computing in Python”. *Nat. Methods* **17**, 261–272 (2020). [arXiv:1907.10121](https://arxiv.org/abs/1907.10121).
- [29] Bergholm et al. “PennyLane: Automatic differentiation of hybrid quantum-classical computations” (2018). [arXiv:1811.04968](https://arxiv.org/abs/1811.04968).
- [30] Korbinian Kottmann, David Wierichs, Guillermo Alonso-Linaje, and Nathan Killoran (2026). code: [XanaduAI/flagsynth](https://github.com/XanaduAI/flagsynth).
- [31] David Wierichs. “Unitary synthesis with recursive KAK decompositions”. https://pennylane.ai/qml/demos/tutorial_unitary_synthesis_kak (2025).
- [32] David Wierichs, Korbinian Kottmann, and Nathan Killoran. “Unitary synthesis with optimal brick wall circuits” (2025). [arXiv:2511.16736](https://arxiv.org/abs/2511.16736).
- [33] Vivek V. Shende, Igor L. Markov, and Stephen S. Bullock. “Minimal universal two-qubit controlled-NOT-based circuits”. *Phys. Rev. A* **69**, 062321 (2004). [arXiv:quant-ph/0308033](https://arxiv.org/abs/quant-ph/0308033).
- [34] William R. Clements, Peter C. Humphreys, Benjamin J. Metcalf, W. Steven Kolthammer, and Ian A. Walmsley. “Optimal design for universal multiport interferometers”. *Optica* **3**, 1460–1465 (2016). [arXiv:1603.08788](https://arxiv.org/abs/1603.08788).
- [35] Víctor López Pastor, Jeff Lundeen, and Florian Marquardt. “Arbitrary optical wave evolution with Fourier transforms and phase masks”. *Opt. Express* **29**, 38441–38450 (2021). [arXiv:1912.04721](https://arxiv.org/abs/1912.04721).
- [36] Ulrich Schollwöck. “The density-matrix renormalization group in the age of matrix product states”. *Annals of Physics* **326**, 96–192 (2011). [arXiv:1008.3477](https://arxiv.org/abs/1008.3477).
- [37] E. Anderson, Z. Bai, C. Bischof, S. Blackford, J. Demmel, J. Dongarra, J. Du Croz, A. Greenbaum, S. Hammarling, A. McKenney, and D. Sorensen. “LAPACK users’ guide”. Society for Industrial and Applied Mathematics. Philadelphia, PA (1999). Third edition. url: <https://www.netlib.org/lapack/lug/>.
- [38] David Wierichs. “Diagonal unitary decomposition”. <https://pennylane.ai/compilation/diagonal-unitary-decomp> (2025).
- [39] David Wierichs. “Phase gradient”. <https://pennylane.ai/compilation/phase-gradient> (2025).
- [40] Mikko Möttönen, Juha J. Vartiainen, Ville Bergholm, and Martti M. Salomaa. “Transformation of quantum states using uniformly controlled rotations”. *Quantum Info. Comput.* **5**, 467–473 (2005). [arXiv:quant-ph/0407010](https://arxiv.org/abs/quant-ph/0407010).
- [41] David Wierichs. “Select-U(2) decomposition”. <https://pennylane.ai/compilation/select-u2-decomp> (2025).
- [42] Korbinian Kottmann. “Introducing matrix product states for quantum practitioners”. https://pennylane.ai/qml/demos/tutorial_mps (2024).
- [43] Hartmut Führ and Ziemowit Rzeszutnik. “A note on factoring unitary matrices”. *Linear Algebra Appl.* **547**, 32–44 (2018).
- [44] Guillermo Alonso and Juan Miguel Arrazola. “Intro to quantum read-only memory (QROM)”. https://pennylane.ai/qml/demos/tutorial_intro_qrom (2024).
- [45] Ryan Babbush, Craig Gidney, Dominic W. Berry, Nathan Wiebe, Jarrod McClean, Alexandru Paler, Austin Fowler, and Hartmut Neven. “Encoding Electronic Spectra in Quantum Circuits with Linear T Complexity”. *Phys. Rev. X* **8**, 041015 (2018). [arXiv:1805.03662](https://arxiv.org/abs/1805.03662).
- [46] Yuval R. Sanders, Dominic W. Berry, Pedro C.S. Costa, Louis W. Tessler, Nathan Wiebe, Craig Gidney, Hartmut Neven, and Ryan Babbush. “Compilation of Fault-Tolerant Quantum Heuristics for Combinatorial Optimization”. *PRX Quantum* **1**, 020312 (2020). [arXiv:2007.07391](https://arxiv.org/abs/2007.07391).
- [47] Dominic W. Berry, Craig Gidney, Mario Motta, Jarrod R. McClean, and Ryan Babbush. “Qubitization of Arbitrary Basis Quantum Chemistry Leveraging Sparsity and Low Rank Factorization”. *Quantum* **3**, 208 (2019). [arXiv:1902.02134](https://arxiv.org/abs/1902.02134).
- [48] Guillermo Alonso-Linaje. “Swap network”. <https://pennylane.ai/compilation/swap-network> (2026).
- [49] Stephen S Bullock and Igor L Markov. “Asymptotically optimal circuits for arbitrary n-qubit diagonal computations”. *Quantum Information and Computation* **4**, 027–047 (2004). [arXiv:quant-ph/0303039](https://arxiv.org/abs/quant-ph/0303039).
- [50] Yumi Nakajima, Yasuhito Kawano, and Hiroshi Sekigawa. “A new algorithm for producing quantum circuits using KAK decompositions”. *Quantum Info. Comput.* **6**, 67–80 (2006). [arXiv:quant-ph/0509196](https://arxiv.org/abs/quant-ph/0509196).
- [51] Brian D Sutton. “Computing the complete CS decomposition”. *Numerical Algorithms* **50**, 33–65 (2009). [arXiv:0707.1838](https://arxiv.org/abs/0707.1838).
- [52] Mehmet Dağlı, Domenico D’Alessandro, and Jonathan D.H. Smith. “A general framework for recursive decompositions of unitary quantum evolutions”. *Journal of Physics A: Mathematical and Theoretical* **41**, 155302 (2008). [arXiv:quant-ph/0701193](https://arxiv.org/abs/quant-ph/0701193).
- [53] Domenico D’Alessandro and Raffaele Romano. “Decompositions of unitary evolutions and entanglement dynamics of bipartite quantum systems”. *J. Math. Phys.* **47** (2006). [arXiv:quant-ph/0603061](https://arxiv.org/abs/quant-ph/0603061).
- [54] Domenico D’Alessandro and Francesca Albertini. “Quantum symmetries and Cartan decompositions in arbitrary dimensions”. *J. Phys. A: Math. Theor.* **40**, 2439 (2007). [arXiv:quant-ph/0504044](https://arxiv.org/abs/quant-ph/0504044).
- [55] Vivek V. Shende and Igor L. Markov. “Quantum circuits for incompletely specified two-qubit operators”. *Quantum Info. Comput.* **5**, 49–57 (2005). [arXiv:quant-ph/0401162](https://arxiv.org/abs/quant-ph/0401162).

Appendix A: Implementation details

Here we discuss the implementation of the various algorithmic components for the recursive flag decomposition and selective de-multiplexing. We follow a top-down approach, starting with the coarse-grained building blocks and working our way down to base cases of the used recursions. The implementation can be found in the `flagsynth` github repository [30].

1. Main algorithms

First, we show in Alg. 1 the core recursive decomposition of (multiplexed) multi-qubit operators. We use it as the recursive flag decomposition for phase gradient implementations, described in Sec. III, and as a subroutine in selective de-multiplexing, described in Sec. IV.

We distinguish two base cases when the recursion reaches either a single qubit or two-qubit unitaries, indicated by $n_b \in \{1, 2\}$; see Alg. 5 below. CSD is the cosine-sine decomposition, the output of which is processed through a recursive call to `CORE_DECOMP` in Alg. 1. `BALANCE_DIAGONAL` implements Eq. (13) and `MUX` simply refers to attaching multiplexer nodes to a pair of gate sequences, effectively merging them into a single gate sequence. $\nabla(\theta_Z, \theta_Y, c, t)$ denotes a multiplexed single-qubit flag with angles $\theta_{Y,Z}$, multiplexing qubits c and target qubit t . $\kappa \in \{\text{True}, \text{False}\}$ encodes whether we break down multiplexed single-qubit gates via `DEC_MUX_1QF`, which is described in App. C2 and is used for SDM. We do not define the sub-diagonals $\Delta_2^{(i,j)}$ but refer to the implementation for details [30]. We use \cup to denote list concatenation, and Pythonic slicing notation.

Algorithm 1 The recursive flag decomposition of (multiplexed) multi-qubit operators. See the appendix text for details about notation and used subroutines.

```

1: procedure CORE_DECOMP( $\{V_i \in U(2^{n-k}) \mid 0 \leq i < 2^k\}$ ,  $q_{\text{mux}} \in \mathbb{Z}^k$ ,  $q_{\text{targ}} \in \mathbb{Z}^{n-k}$ ,  $n_b \in \{1, 2\}$ ,  $\kappa \in \{0, 1\}$ )
2:   if  $n - k = n_b$  then
3:     if  $n_b = 1$  then
4:        $F_i, \Delta_i \leftarrow \text{ONE\_QUBIT\_FLAG}(V_i, q_{\text{targ}})$ 
5:     else
6:        $F_i, \Delta_i \leftarrow \text{TWO\_QUBIT\_FLAG}(V_i, q_{\text{targ}})$ 
7:     end if
8:      $F \leftarrow \text{MUX}(\{F_i\}, q_{\text{mux}})$ 
9:      $\Delta \leftarrow \bigoplus_{i=0}^{2^k-1} \Delta_i$ 
10:    if  $\kappa$  then
11:       $F, \tilde{\Delta} \leftarrow \text{DEC\_MUX\_1QF}(F)$ 
12:       $\Delta \leftarrow \Delta \cdot \tilde{\Delta}$ 
13:    end if
14:    return  $F, \Delta$ 
15:  end if
16:   $K_{00}^{(i)}, K_{01}^{(i)}, \theta_Y^{(i)}, K_{10}^{(i)}, K_{11}^{(i)} \leftarrow \text{CSD}(V_i)$ 
17:   $q'_{\text{mux}} \leftarrow q_{\text{mux}} \cup q_{\text{targ}, [1]}$ 
18:   $q'_{\text{targ}} \leftarrow q_{\text{targ}, [1]}$ 
19:   $F_1, \Delta_1 \leftarrow \text{CORE\_DECOMP}(\{K_{1j}^{(i)}\}, q'_{\text{mux}}, q'_{\text{targ}}, n_b, \kappa)$ 
20:   $\theta_Z, \Delta_2 \leftarrow \text{BALANCE\_DIAGONAL}(\Delta_1, k)$ 
21:   $F_A \leftarrow \nabla(\theta_Z, \theta_Y, q_{\text{mux}} \cup q'_{\text{targ}} \cup q_{\text{targ}, [1]})$ 
22:   $\Delta_2 \leftarrow \Delta_2 \otimes_k (1, 1)$ 
23:  if  $\kappa$  then
24:     $F_A, \tilde{\Delta} \leftarrow \text{DEC\_MUX\_1QF}(F_A)$ 
25:     $\Delta_2 \leftarrow \Delta_2 \cdot \tilde{\Delta}$ 
26:  end if
27:   $K_{0j}^{(i)} \leftarrow K_{0j}^{(i)} \cdot \Delta_2^{(i,j)}$ 
28:   $F_0, \Delta_0 \leftarrow \text{CORE\_DECOMP}(\{K_{0j}^{(i)}\}, q'_{\text{mux}}, q'_{\text{targ}}, n_b, \kappa)$ 
29:  return  $F_1 \cup F_A \cup F_0, \Delta_0$ 
30: end procedure

```

Next, we show in Alg. 2 the SDM algorithm described in Sec. IV. It uses a standard two-qubit decomposition `TWO_QUBIT_DECOMP` with 15 rotations and 3 CNOTs as base case, Eq. (32). `DE_MUX` de-multiplexes a 1-multiplexed unitary—see Eq. (27)—`REC_FLAG_DEC` is given in Alg. 3 below, and `MÖTTÖNEN` implements the

Möttönen decomposition (see Eq. (D.2)), symmetrized according to the last argument to the right or left. To enable the symmetrization, we need to re- and de-multiplex the central two unitaries via `RE_DE_MUX`. This is a combination of simple matrix multiplication and `DE_MUX`; see the implementation in [30] for more details.

Algorithm 2 SDM algorithm using an adapted recursive flag decomposition, see Alg. 3, and symmetrized Möttönen decompositions. See the appendix text for more details.

```

1: procedure SDM( $V \in U(2^n)$ ,  $q, n \geq 2$ )
2:   if  $n = 2$  then
3:     return TWO_QUBIT_DECOMP( $V$ )
4:   end if
5:    $K_{00}, K_{01}, \theta_Y, K_{10}, K_{11} \leftarrow \text{CSD}(V)$ 
6:    $M_{10}, \theta_Z^{(1)}, M_{11} \leftarrow \text{DE\_MUX}(K_{10}, K_{11})$ 
7:    $M_{00}, \theta_Z^{(0)}, M_{01} \leftarrow \text{DE\_MUX}(K_{00}, K_{01})$ 
8:    $M'_{01}, \theta'_Y, M'_{10} \leftarrow \text{RE\_DE\_MUX}(M_{01}, M_{10}, \theta_Y, q)$ 
9:    $q' \leftarrow q_{[1]}$ 
10:   $F_{11}, \Delta_{11} \leftarrow \text{REC\_FLAG\_DEC}(M_{11}, q', n_b = 2)$ 
11:   $F_{10}, \Delta_{10} \leftarrow \text{REC\_FLAG\_DEC}(M'_{10} \cdot \Delta_{11}, q', n_b = 2)$ 
12:   $F_{01}, \Delta_{01} \leftarrow \text{REC\_FLAG\_DEC}(M'_{01} \cdot \Delta_{10}, q', n_b = 2)$ 
13:   $U_{00} \leftarrow \text{SDM}(M_{00} \cdot \Delta_{01}, q')$ 
14:   $C_{Z,1} = \text{MÖTTÖNEN}(\theta_Z^{(1)}, q', q_0, Z, \text{sym} = R)$ 
15:   $C_Y = \text{MÖTTÖNEN}(\theta'_Y, q', q_0, Z, \text{sym} = R)$ 
16:   $C_{Z,0} = \text{MÖTTÖNEN}(\theta_Z^{(0)}, q', q_0, Z, \text{sym} = L)$ 
17:  return  $F_{11} \cup C_Z^{(1)} \cup C_{10} \cup C_Y \cup C_{01} \cup C_Z^{(0)} \cup C_{00}$ 
18: end procedure

```

Next, Alg. 3 shows the adapted recursive flag decomposition that we use in the previous SDM algorithm. It combines calls to itself and to the first variant of the (multiplexed) flag decomposition in Alg. 1. Other subroutines are the same as used above in SDM. The modified matrices \tilde{K}_{0j} result from the re- and de-multiplexing step and the CZ gate to be absorbed from the symmetrized Möttönen decomposition of the R_Y multiplexer.

Algorithm 3 Recursive flag decomposition adjusted to be used in SDM (Alg. 2).

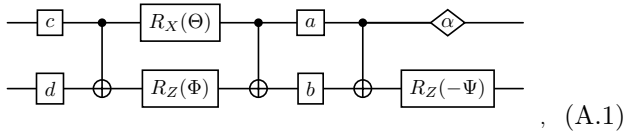
```

1: procedure REC_FLAG_DEC( $V \in U(2^n), q, n_b$ )
2:   if  $n = n_b = 1$  then
3:     return ONE_QUBIT_FLAG( $V, q$ )
4:   else if  $n = n_b = 2$  then
5:     return TWO_QUBIT_FLAG( $V, q$ )
6:   end if
7:    $K_{00}, K_{01}, \theta_Y, K_{10}, K_{11} \leftarrow \text{CSD}(V)$ 
8:    $M_{10}, \theta_Z^{(1)}, M_{11} \leftarrow \text{DE\_MUX}(K_{10}, K_{11})$ 
9:    $q' \leftarrow q_{[1:]}$ 
10:   $F_{11}, \Delta_{11} \leftarrow \text{REC\_FLAG\_DEC}(M_{11}, q', n_b)$ 
11:   $F_{11}, \tilde{\Delta} \leftarrow \text{DEC\_MUX\_1QF}(F_{11})$ 
12:   $\Delta_{11} \leftarrow \Delta_{11} \cdot \tilde{\Delta}$ 
13:   $C_{Z,1} = \text{MÖTTÖNEN}(\theta_Z^{(1)}, q', q_0, Z, \text{sym} = R)$ 
14:   $M_{00}, \theta_Z^{(0)}, M_{01} \leftarrow \text{DE\_MUX}(K_{00}, K_{01})$ 
15:   $M'_{01}, \theta_Y, M'_{10} \leftarrow \text{RE\_DE\_MUX}(M_{01}, M_{10}, \theta_Y, q)$ 
16:   $F_{10}, \Delta_{10} \leftarrow \text{REC\_FLAG\_DEC}(M'_{10} \cdot \Delta_{11}, q', n_b)$ 
17:   $F_{10}, \tilde{\Delta} \leftarrow \text{DEC\_MUX\_1QF}(F_{10})$ 
18:   $\Delta_{10} \leftarrow \Delta_{10} \cdot \tilde{\Delta}$ 
19:   $C_Y = \text{MÖTTÖNEN}(\theta_Y, q', q_0, Y, \text{sym} = R)$ 
20:   $\tilde{K}_{00} = M_{00} \cdot \exp(-\frac{i}{2}\theta_Z^{(0)}) \cdot M'_{01} \cdot \Delta_{10}$ 
21:   $\tilde{K}_{01} = M_{00} \cdot \exp(\frac{i}{2}\theta_Z^{(0)}) \cdot M'_{01} \cdot Z_0 \cdot \Delta_{10}$ 
22:   $F_0, \Delta \leftarrow \text{CORE\_DECOMP}(\{\tilde{K}_{00}, \tilde{K}_{01}\}, q_0, q_{[1:]}, n_b, 1)$ 
23:  return  $F_{11} \cup C_{Z,1} \cup F_{10} \cup C_Y \cup F_0, \Delta$ 
24: end procedure

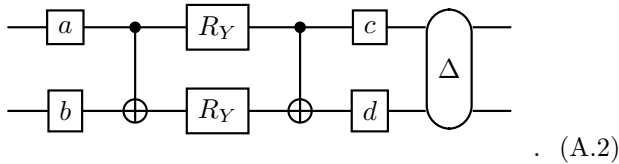
```

2. Base case algorithms

With the main algorithmic building blocks covered, we now turn to the base case algorithms used above, beginning with the base case $n_b = 2$ flag decomposition. The solution is based on [33, Thm. VI.3], given by:



where $a, b, c, d \in SU(2)$, the diamond-shaped gate denotes a global phase $e^{i\alpha}$, and we report the adjoint of the original decomposition in order to move the diagonal Δ to the right rather than the left later on. This decomposition is used by [1, Thm. 14] to arrive at the two-qubit template



These references prove the existence of the “asymmetric” decomposition Eq. (A.1) and the decomposition up to a diagonal in Eq. (A.2) constructively, only requiring standard linear algebra tools like matrix multiplication,

eigenvalue decomposition¹⁶ and computing determinants. We implemented the asymmetric decomposition method in `flagsynth.asymmetric_two_qubit_decomp` and summarize its algorithm for convenience in Alg. 4.

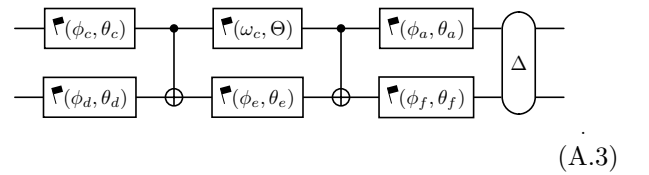
Algorithm 4 Computing the variables for Eq. (A.1). We do not explicitly explain the algorithms detailed in [33, Props. V.2, IV.3].

```

1: procedure ASYMMETRIC_DECOMP( $V \in U(4)$ )
2:    $V \leftarrow \text{CNOT} \cdot V$ 
3:    $\alpha \leftarrow \frac{1}{4} \arg(\det(V))$ 
4:    $V \leftarrow V e^{-i\alpha}$ 
5:    $\Psi, \Theta, \Phi \leftarrow \text{Prop.V2}(V)$ 
6:    $V' \leftarrow \text{Ad}_{\text{CNOT}}(R_Z^{(1)}(\Psi)) \cdot V$ 
7:    $W \leftarrow \text{Ad}_{\text{CNOT}}(R_X^{(0)}(\Theta)R_Z^{(1)}(\Phi))$ 
8:    $a, b, c, d \leftarrow \text{Prop.IV.3}(V', W)$ 
9:   return  $a, b, c, d, \alpha, \Psi, \Theta, \Phi$ 
10: end procedure

```

The decomposition in [1] yields a constructive description of the two-qubit flag decomposition, but with only two degrees of freedom—that of an Ising-interaction rotation R_{ZZ} , and that of the global phase—in the diagonal. In order to arrive at the flag decomposition with the stated numbers of degrees of freedom, we perform a combination of Euler decompositions and basis transformations of the single-qubit operators, and commute R_Z gates through (temporarily created) CZ gates. This ultimately allows us to absorb two R_Z rotations into Δ , yielding $2^n = 2^2 = 4$ degrees of freedom in Δ and $4^n - 2^n = 16 - 4 = 12$ degrees of freedom in the remaining flag circuit. We implemented the technique from [1, Thm. 14] together with this postprocessing step in `flagsynth.two_qubit_flag` (see Alg. 5), which will be used by Alg. 1. The returned variables are to be used in a circuit as follows:



Here we used repeated basis changes via rotations about Y or Z with angles $\pm \frac{\pi}{2}$ to modify the circuit obtained from Euler decompositions into the shown regular arrangement of single-qubit flags.

¹⁶ Strictly speaking, we require eigenvalue decompositions of symmetric unitary matrices into real eigenbases. Those can be achieved either through modification of a standard eigenvalue decomposition [43] or through simultaneous diagonalization of the real and imaginary parts.

Algorithm 5 One-qubit and two-qubit flag decompositions. $\mathbb{V}(\theta_Z, \theta_Y, q)$ denotes a single-qubit flag with angles $\theta_{Y,Z}$ acting on qubit q . The subroutine ASYMMETRIC_DECOMP is described in Alg. 4, and EULER is the standard ZYZ Euler decomposition. See Eq. (A.3) for the usage of the computed variables.

```

1: procedure ONE_QUBIT_FLAG( $V \in U(2), q \in \mathbb{Z}$ )
2:    $\theta_Z, \theta_Y, \omega, \phi \leftarrow \text{EULER}(V)$ 
3:    $F \leftarrow \mathbb{V}(\theta_Z, \theta_Y, q)$ 
4:    $\Delta \leftarrow (e^{-i(\phi+\omega/2)}, e^{-i(\phi-\omega/2)})$ 
5:   return  $F, \Delta$ 
6: end procedure
7: procedure TWO_QUBIT_FLAG( $V \in U(4), q \in \mathbb{Z}^2$ )
8:    $a, b, c, d, \alpha, \Psi, \Theta, \Phi \leftarrow \text{ASYMMETRIC\_DECOMP}(V)$ 
9:    $\phi_a, \theta_a, \omega_a \leftarrow \text{EULER}(a)$ 
10:   $\phi_c, \theta_c, \omega_c \leftarrow \text{EULER}(c)$ 
11:   $\phi_d, \theta_d, \omega_d \leftarrow \text{EULER}(R_Y(-\frac{\pi}{2}) \cdot d)$ 
12:   $\phi_e, \theta_e, \omega_e \leftarrow \text{EULER}(R_X(-\Phi) \cdot R_Z(\omega_d))$ 
13:   $\phi_f, \theta_f, \omega_f \leftarrow \text{EULER}(b \cdot R_X(\omega_e) \cdot R_Y(\frac{\pi}{2}))$ 
14:   $F, \Delta \leftarrow \text{CONVERT\_TO\_FLAGS}(C)$ 
15:   $\omega_c \leftarrow \omega_c + \frac{\pi}{2}$ 
16:   $\phi_a \leftarrow \phi_a - \frac{\pi}{2}$ 
17:   $\Delta \leftarrow \text{diag}(R_Z^{(0)}(\omega_a) \cdot R_Z^{(1)}(\omega_f) \cdot R_{ZZ}(\Psi)e^{i\alpha})$ 
18:  return  $\phi_c, \theta_c, \phi_d, \theta_d, \omega_c, \Theta, \phi_e, \theta_e, \phi_a, \theta_a, \phi_f, \theta_f, \Delta$ 
19: end procedure

```

Appendix B: Resource counts for phase gradient decompositions

Here we collect decompositions and implementation details for the phase gradient decomposition of our unitary synthesis and MPS preparation circuits.

1. QROM cost

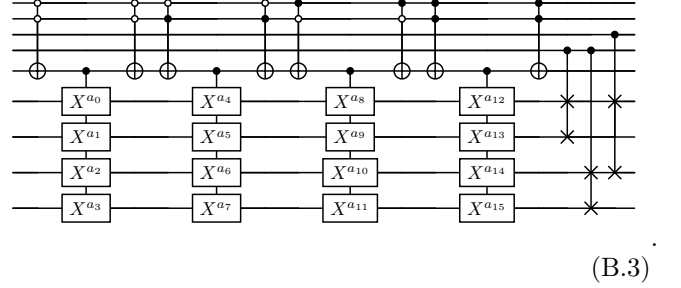
The Quantum Read-Only Memory (QROM) is an operator that stores bitstrings of size b , each associated with a unique index, such that

$$\text{QROM} |i\rangle |0\rangle = |i\rangle |a_i\rangle, \quad (\text{B.1})$$

where each $a_i \in \{0,1\}^b$ denotes a classical bitstring. Throughout this work, following [21], we adopt a resource-efficient variant of QROM that reduces overall cost by forgoing the uncomputation of auxiliary qubits. Specifically, the QROM operator acts as

$$\text{QROM} |i\rangle |0\rangle |0\rangle = |i\rangle |a_i\rangle |v_i\rangle, \quad (\text{B.2})$$

where $|v_i\rangle$ is an auxiliary state whose content is irrelevant to the computation. The decomposition introduced in [16] follows the *SelectSwap* structure, illustrated below:



In this circuit, the first four qubits represent the input state $|x\rangle$. The fifth qubit is an auxiliary qubit used in the decomposition process. The following register corresponds to the target qubits, where we aim to load the bitstring $|a_x\rangle$. The remaining registers consist of additional auxiliary qubits used throughout the computation.

This technique, described in [44], distributes the loading of bitstrings across a two-dimensional memory layout. It partitions the control register into two sets: the first set determines the column in which the bitstring $|a_i\rangle$ resides, while the second set identifies the corresponding row.

As depicted in the circuit, the QROM operator is divided into two main components. The Select block loads a full column of bitstrings and stores them across the target and auxiliary registers. For example, for the specific case $|i\rangle = |14\rangle$, the operator acts as

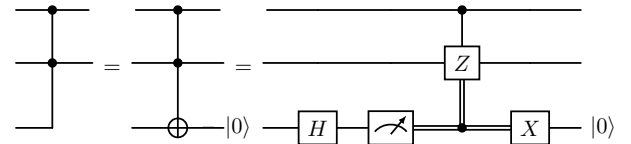
$$\text{Select} |14\rangle |0\rangle (|0\rangle |0\rangle |0\rangle) = |14\rangle |a_{12}\rangle (|a_{13}\rangle |a_{14}\rangle |a_{15}\rangle),$$

where the relevant bitstring $|a_{14}\rangle$ has been loaded, but not in the target position. The SwapUp block then reorders the bitstrings such that $|a_{14}\rangle$ is brought to the target register,

$$\text{SwapUp} |14\rangle |a_{12}\rangle (|a_{13}\rangle |a_{14}\rangle |a_{15}\rangle) = |14\rangle |a_{14}\rangle (|v_{14}\rangle),$$

where $|v_{14}\rangle$ denotes a reordered product of the remaining bitstrings, which are no longer used.

To implement the Select block efficiently, [45] introduced a construction based on TemporaryAnd gates. It was shown that a QROM storing 2^n entries can be implemented using $2^n - 1$ Toffoli gates. TemporaryAnd gates are a resource-saving alternative to standard Toffoli gates. They simulate the AND of two control qubits by temporarily storing the result in an auxiliary qubit. These additional qubits are uncomputed later using only Clifford operations, which reduces the overall cost without sacrificing reversibility:



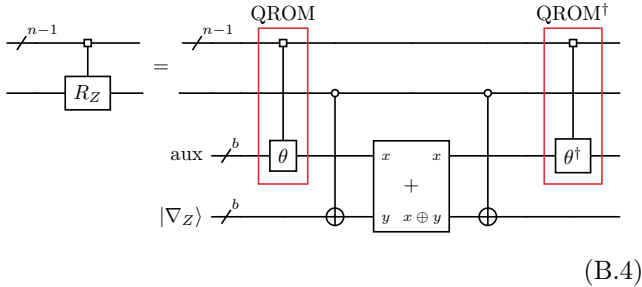
The cost of the SelectSwap decomposition depends on the parameter Λ , which specifies the number of rows used to arrange the bitstrings. Accordingly, the control register is split into two parts: $\log_2(\Lambda)$ qubits for the controlled-Swap operations in the SwapUp block, and $\log_2(2^n/\Lambda)$ qubits for the Select block.

Given this structure, the Select block requires $2^n/\Lambda - 1$ Toffoli gates, as it acts over a reduced address space, and the SwapUp block requires $b(\Lambda - 1)$ Toffoli gates, since each controlled-Swap can be implemented using one Toffoli and two CNOT gates. Hence, the total Toffoli cost of the QROM implementation is given by:

$$C_{\text{QROM}} = \frac{2^n}{\Lambda} + (\Lambda - 1)b - 1.$$

2. QROM-based decomposition of R_Z multiplexer

The R_Z rotation multiplexer can be decomposed using a QROM, an adder, and a sequence of CNOT gates. This decomposition is illustrated in the following circuit, where we introduce an auxiliary b -qubit register onto which the angles are loaded, and another b -qubit register that carries a phase gradient state $|\nabla_Z\rangle$:



(B.4)

Here we are using a phase gradient resource state $|\nabla_Z\rangle = \frac{1}{\sqrt{2^b}} \sum_{k=0}^{2^b-1} e^{-2\pi i k/2^b} |k\rangle$, and b denotes the number of bits used to represent the rotation angles of the multiplexer in binary. The circuit leverages the following key properties¹⁷:

- (0) $\text{Add} |x\rangle |y\rangle = |x\rangle |x + y\rangle$
- (1) $\text{Add} |x\rangle |\nabla_Z\rangle = e^{2\pi i x/2^b} |x\rangle |\nabla_Z\rangle$
- (2) $(I \otimes X) \text{Add}(I \otimes X) |x\rangle |y\rangle = |x\rangle |y - x\rangle$
- (3) $(I \otimes X) \text{Add}(I \otimes X) |x\rangle |\nabla_Z\rangle = e^{-2\pi i x/2^b} |x\rangle |\nabla_Z\rangle$

Property (0) is simply the definition of the Add operator, which can be used to derive property (1). This shows how specific phases can be applied using basic arithmetic.

Another fundamental identity is property (2), which demonstrates that conjugating the Add with Pauli-X gates on the target register effectively performs a subtraction. This can be proven by observing that applying an X gate to $|y\rangle$ produces $|1 - y\rangle$. After applying the addition, the target register becomes $|1 - y + x\rangle$, and applying X again yields $|y - x\rangle$. Using this identity, we can derive property (3), which shows that the negative phase can be introduced by conjugating the Add with X gates when the target is in the state $|\nabla_Z\rangle$.

Using the properties described above, we can now demonstrate the equivalence between the arithmetic-based construction and the direct application of multiplexed R_Z rotations. Assume we begin with an initial state of the form $\sum_i \alpha_i |i\rangle |\psi\rangle$, and our goal is to obtain the state

$$\sum_i \alpha_i |i\rangle R_Z(\theta_i) |\psi\rangle.$$

To achieve this, we employ a QROM to load the binary-encoded values of $\frac{2^b \theta_i}{4\pi}$ into an auxiliary register. That is, we prepare the state

$$\sum_i \alpha_i |i\rangle |\psi\rangle \left| \frac{2^b \theta_i}{4\pi} \right\rangle.$$

Let us write the data qubit as $|\psi\rangle = \beta |0\rangle + \gamma |1\rangle$. By applying the X gates in the target register controlled on the data qubit, we perform an addition when the data qubit is in $|1\rangle$, and a subtraction when it is in $|0\rangle$. This results in the state

$$\sum_i \alpha_i |i\rangle \left(e^{-2\pi i \left(\frac{2^b \theta_i}{4\pi}\right)/2^b} \beta |0\rangle + e^{2\pi i \left(\frac{2^b \theta_i}{4\pi}\right)/2^b} \gamma |1\rangle \right) \left| \frac{2^b \theta_i}{4\pi} \right\rangle.$$

Simplifying the phase terms, we obtain

$$\sum_i \alpha_i |i\rangle \left(e^{-i\theta_i/2} \beta |0\rangle + e^{i\theta_i/2} \gamma |1\rangle \right) \left| \frac{2^b \theta_i}{4\pi} \right\rangle.$$

Finally, we uncompute on the final register, restoring it to $|0\rangle$, and leaving the state

$$\sum_i \alpha_i |i\rangle R_Z(\theta_i) |\psi\rangle,$$

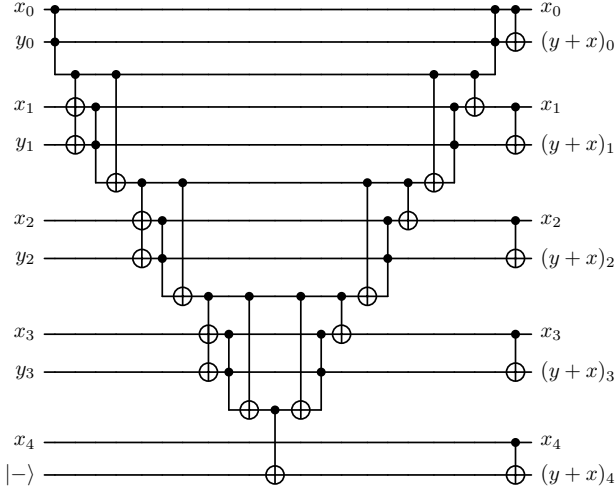
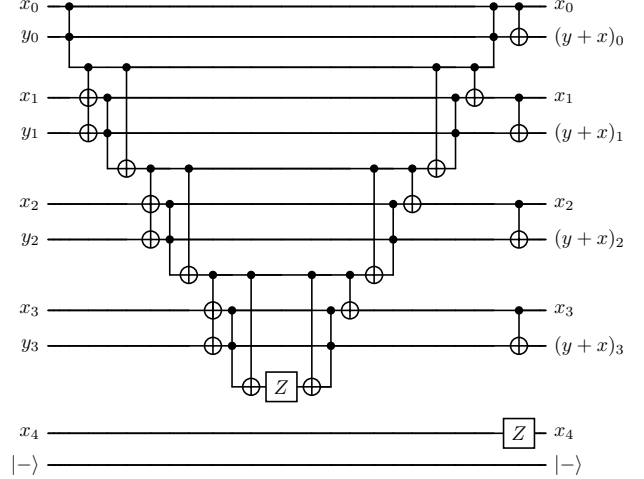
which is exactly the transformation we aimed to implement. More information on this technique can be found in the PennyLane compilation hub [39].

3. Adder Operator

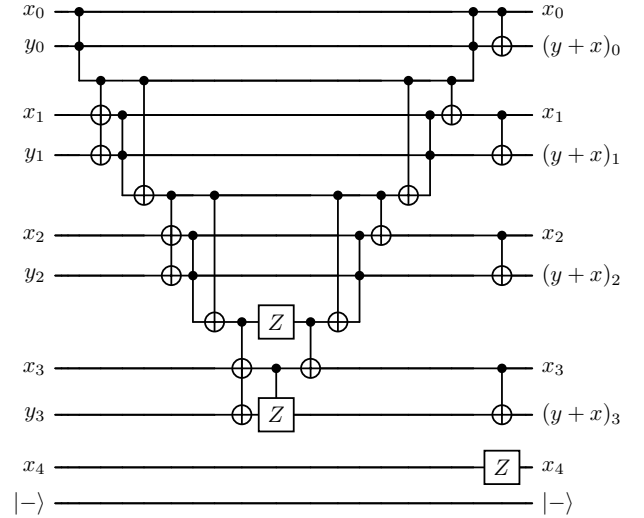
The adder operator, defined as $\text{Add} |x\rangle |y\rangle = |x\rangle |y + x\rangle$, is a well-studied operation, with notable implementations such as in [17], where the decomposition

¹⁷ Note that the two sub-systems considered here correspond to the auxiliary qubits and those carrying the phase gradient state in Eq. (B.4). In particular, we write $(I \otimes X) := (I^{\otimes b} \otimes X^{\otimes b})$ for brevity.

relies on the use of TemporaryAnd operators. In our analysis, we count each TemporaryAnd as a Toffoli gate, as it performs an equivalent logical function. However, we do not count the uncomputation of TemporaryAnd, since it can be implemented using only Clifford gates and measurements. In the decomposition shown below, for the case of adding numbers with $b = 5$ digits, it can be observed that $(b - 1)$ Toffoli gates are required:



Finally, as presented in [17], the circuit can be simplified by removing one of the TemporaryAnds:



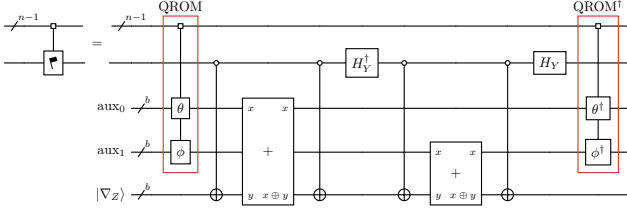
We see how this realizes the operation $\text{Add}|x\rangle|y\rangle = |x\rangle|y+x\rangle$ when representing x_0 as the least significant bit of x , and x_4 as the most significant bit. For example, $|x = 3\rangle = |x_4x_3x_2x_1x_0\rangle = |00011\rangle$. Note that in the qubit y_4 , we take the input state to be $|-\rangle$. This simplification comes because of two helpful observations. First, for our usage, the second input register will always contain a phase gradient state, i.e., $|y_4y_3y_2y_1y_0\rangle = |\nabla_Z\rangle$. Second, the most significant wire of a phase gradient state will always be in a $|-\rangle$ state, regardless of size. This allows for a simplification of the adder circuit, as there are two CNOT gates targeting this wire. When these are activated, they effectively flip the sign of the state, which is equivalent to replacing the CNOT gates with a single Z gate acting on the control qubits:

In aggregate, the Toffoli gate cost is reduced to $(b - 2)$, a value that will be used throughout this work, and also used in [46].

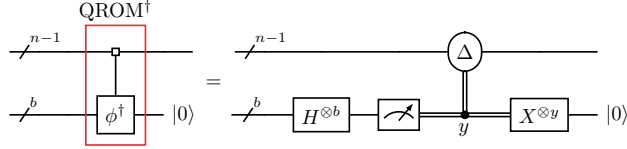
4. Multiplexer of 1-qubit flag operators

In this section, we introduce the decomposition of single-qubit flag-operator multiplexers, that is, multiplexers over gates of the form $R_Y(\phi) \cdot R_Z(\theta)$. To this end, we exploit the identity $R_Y = H_Y R_Z H_Y^\dagger$, where $H_Y = S H$, together with the decomposition of the R_Z multiplexer derived in the previous section. The main idea is to load, in parallel, the binary representations of θ and ϕ using a QROM. Then, two adders are applied between these representations together with a phase

gradient resource, followed by an uncomputation of the QROM:



The last operation, QROM^\dagger , corresponds to reversing the action described in Eq. (B.2). We can achieve this by measuring all target qubits on the auxiliary register in the X basis and, based on the measurement outcomes, applying phase corrections to the control qubits:



Here, $X^{\otimes y} = \bigotimes_j X^{y_j}$ is a shorthand notation for applying X whenever the measurement result $y_j = 1$ on the respective qubit to reset it to $|0\rangle$.

Our goal here is to map any input state $|i\rangle |\phi_i\rangle |\psi_i\rangle$ back to $|i\rangle |0\rangle |\psi_i\rangle$, where $|\phi_i\rangle$ is the i th QROM bitstring and $|\psi_i\rangle$ is an arbitrary state that may be entangled with these qubits.

Measuring the auxiliary qubits in the X basis is equivalent to applying a Hadamard gate followed by a measurement in the Z basis. After applying the Hadamard gate, the system evolves into the state¹⁸

$$\sum_i \alpha_i |i\rangle \left(\frac{1}{\sqrt{2^b}} \sum_x (-1)^{\phi_i \odot x} |x\rangle \right) |\psi_i\rangle.$$

Assuming that the measurement yields the bitstring $|y\rangle$, the post-measurement state becomes

$$\sum_i \alpha_i (-1)^{\phi_i \odot y} |i\rangle |y\rangle |\psi_i\rangle.$$

Therefore, by uncomputing the register containing $|y\rangle$ (e.g., using X gates), and applying a diagonal operator Δ such that $\Delta_{ii} = (-1)^{\phi_i \odot y}$, we obtain the desired state¹⁹.

The diagonal operator Δ consists of ± 1 entries, which allows it to be merged with the subsequent multiplexers in the circuit. For this reason, we do not account for

its cost within this block. Based on this, the cost of the flag multiplexers consists of the initial QROM (using $2b$ target qubits and $n - 1$ control qubits), together with two adders, each with cost $b - 2$, as detailed in App. B.3. This results in a total cost of:

$$\left(\frac{2^{n-1}}{\Lambda} + (\Lambda - 1)2b - 1 \right) + 2(b - 2) = \frac{2^n}{2\Lambda} + 2\Lambda b - 5.$$

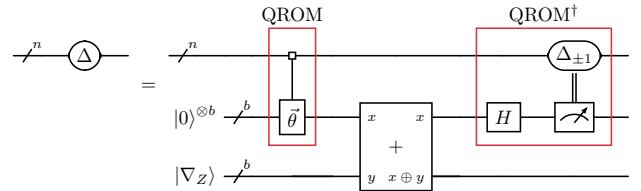
5. Phase gradient decomposition of a diagonal operator

We now want to show how to implement a diagonal operator using a special phase gradient decomposition. We first note that one can identify a diagonal operator as a multiplexed R_Z rotation with an additional qubit initialized in $|0\rangle$ as described in Eq. (40). The same logic applies for an initial state in $|1\rangle$, such that we get

$$\begin{array}{c} \text{---}^n \text{---} \Delta \text{---} \\ = \\ \text{---}^n \text{---} \text{---} \\ |1\rangle \text{---} \text{---} R_Z \text{---} \end{array} \quad (\text{B.5})$$

For diagonal elements $\Delta_{ii} = \exp(i\theta_i)$, the angles of the multiplexed R_Z rotation are given by $2\theta_i$. This equivalence holds because applying the multiplexed R_Z with angles $2\theta_j$ to a basis state $|j\rangle |1\rangle$ yields $|j\rangle R_Z(2\theta_j) |1\rangle = e^{i\theta_j} |j\rangle |1\rangle$ ²⁰. Thus, a diagonal matrix Δ acting on the control qubits such that $\Delta |j\rangle = e^{i\theta_j} |j\rangle$, is equivalent to the multiplexed R_Z rotation with angles $2\theta_j$ in Eq. (B.5).

We can now use Eq. (B.4) to realize the multiplexed R_Z gate and overall obtain



Due to the fixed initial state $|1\rangle$ on the target qubit of the multiplexed R_Z rotation, the two CNOT gates in Eq. (B.4) controlled on the target wire become obsolete. Hence, we can remove the qubit we artificially introduced previously in Eq. (B.5) again.

The diagonal correction in the adjoint QROM consists of ± 1 elements and cannot be merged into any subsequent operation in our unitary synthesis scheme, as the

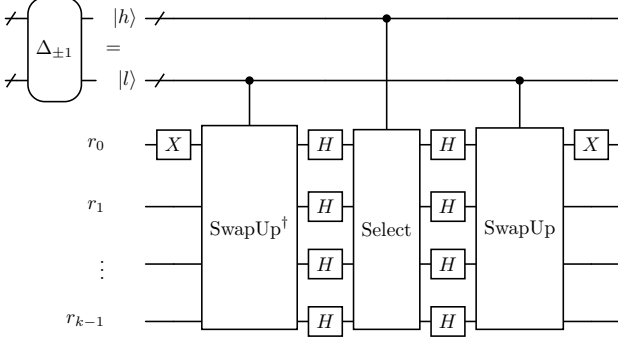
¹⁸ Here, \odot refers to bitwise multiplication.

¹⁹ Auxiliary wires used in the QROM decomposition can also be uncomputed by applying the same measurement trick.

²⁰ Recall that $R_Z(\theta) = e^{-i\frac{\theta}{2}Z} = \text{diag}\left(e^{-i\frac{\theta}{2}}, e^{i\frac{\theta}{2}}\right)$.

full diagonal operator itself appears at the end of the circuit. Therefore, we must describe how to apply the sign corrections. In particular, we will use the circuit introduced in [47], which employs a QROM to store whether a sign correction should be applied to the i th element. This is done by loading a $|1\rangle$ into the target qubit if a correction is needed, or leaving it in the $|0\rangle$ state otherwise.

By leveraging the Select block and the Swap block (also called SwapUp [48]) described in the QROM construction [16], we can implement the sign correction through the circuit identity



where $|h\rangle$ and $|l\rangle$ are the two subsets of wires that define the QROM control wires as described in App. B 1, r_0 is the target qubit used to store the signs, and the remaining qubits r_1, \dots, r_{k-1} are auxiliary qubits used for the encoding and manipulation of the QROM data. In this circuit, the size of the register will always be $b = 1$, since this is enough to store the target sign. Therefore a_i is a single bit instead of a bitstring. To understand the behavior of the circuit, let us assume that all the a_i bits are arranged in a 4×4 matrix in the circuit, distributed in depth and width, as shown in the SelectSwap circuit in Eq. (B.3), and that all auxiliary qubits are initially in the $|0\rangle$ state. Let us walk through an example with $k = 4$ and suppose we input the state $|1110\rangle = |14\rangle$, i.e., $|h\rangle = |11\rangle = |3\rangle$ and $|l\rangle = |10\rangle = |2\rangle$. After applying the first X gate, the state becomes

$$(|h\rangle |l\rangle)(|r_0\rangle |r_1\rangle |r_2\rangle |r_3\rangle) = (|11\rangle |10\rangle)(|1\rangle |0\rangle |0\rangle |0\rangle).$$

Applying the first SwapUp † block places the $|r_0\rangle = |1\rangle$ into the row where a_{14} will be encoded,

$$(|11\rangle |10\rangle)(|0\rangle |0\rangle |1\rangle |0\rangle),$$

which is the second position since $l = 2$. Next, Hadamard gates are applied, yielding the state

$$(|11\rangle |10\rangle)(|+\rangle |+\rangle |-\rangle |+\rangle).$$

When the third column data is loaded ($h = 3$) using the Select block, we apply the operator $X^{a_{12}} \otimes X^{a_{13}} \otimes X^{a_{14}} \otimes X^{a_{15}}$ onto the target register. This yields a negative phase from only the $|-\rangle$ component, as $|+\rangle$ is unaffected by X . Therefore, we obtain

$$(|11\rangle |10\rangle)(|+\rangle |+\rangle (-1)^{a_{14}} |-\rangle |+\rangle).$$

After reapplying Hadamard gates, undoing the SwapUp with SwapUp † , and executing the final X on the first auxiliary qubit, we arrive at

$$(-1)^{a_{14}}(|11\rangle |10\rangle)(|0\rangle |0\rangle |0\rangle |0\rangle).$$

Therefore, the i th bit stored in the QROM determines the sign of the i th element of the diagonal operator.

The cost of the SwapUp block in this construction is $(\Lambda' - 1)$, where Λ' denotes the number of rows used in this QROM (with $b = 1$). The cost of the Select operation is given by $2^n/\Lambda' - 1$, resulting in a total cost for this block of

$$\frac{2^n}{\Lambda'} + \Lambda' - 2.$$

Note that we do not assign any additional cost to the SwapUp † block since, as shown in [47], it can be implemented without Toffoli gates: all Toffolis involved in this uncomputation can be replaced by their corresponding TemporaryAnd adjoints. In App. B 6 we detail this decomposition.

Combining all these components, we deduce that the cost of implementing the diagonal operator consists of three main contributions. The first comes from the initial QROM, which requires

$$\frac{2^n}{2\Lambda} + (2\Lambda - 1)b - 1$$

Toffoli gates. This corresponds to a QROM with 2Λ rows, which is feasible here since we have more qubits available (we do not need to load two angles in parallel).

The second contribution comes from the adder, with cost $b - 2$, and finally, the third contribution comes from the sign-correction block described previously, whose cost is

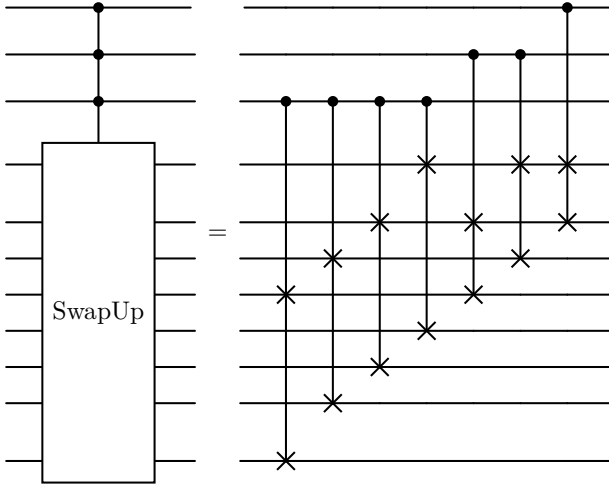
$$\frac{2^n}{\Lambda'} + \Lambda' - 2.$$

Adding these terms together, the total Toffoli cost becomes

$$\frac{2^n}{2\Lambda} + 2\Lambda b + \frac{2^n}{\Lambda'} + \Lambda' - 5.$$

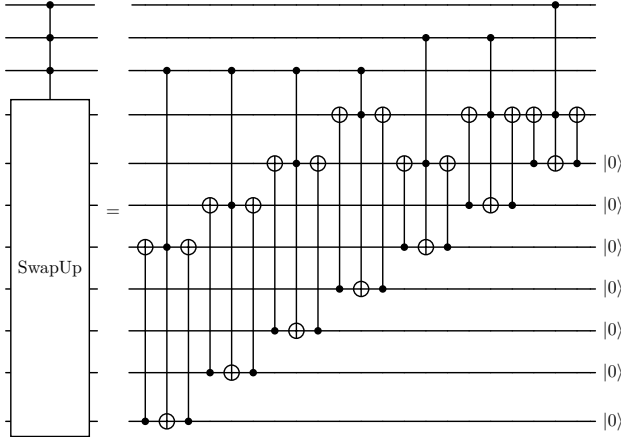
6. Uncomputing Swap block

In the context of the QROM, a SwapUp block is employed to re-arrange a bitstring across auxiliary qubits. This operation is defined as follows:



(B.6)

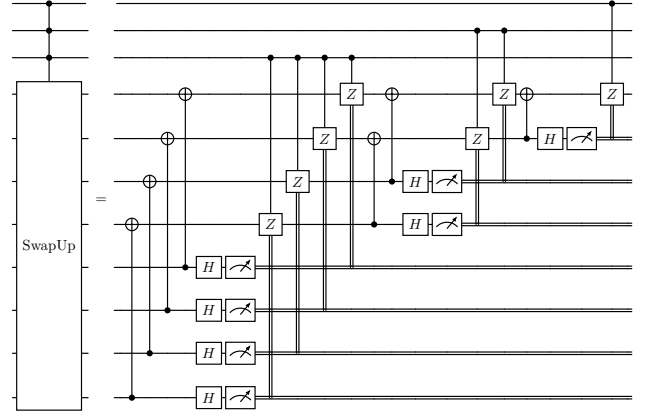
Note that the control nodes on the left-hand side are there to indicate the wires that the right-hand side circuit is controlling on²¹. When this operation is applied at the end of a circuit to uncompute qubits, i.e., we know the output will be $|0\rangle$, it can be implemented without the use of any Toffoli gates. Consider the following decomposition, in which each controlled-Swap gate is expressed solely in terms of CNOT gates and Toffoli gates:



(B.7)

Next, as shown in [47], the CNOT gate after each Toffoli gate can be eliminated, and the Toffoli gates can be replaced by the adjoints of TemporaryAnd operations:

²¹ In particular, the SwapUp box is not a well-defined operation that we control, but rather the box together with the control nodes define the operation.



(B.8)

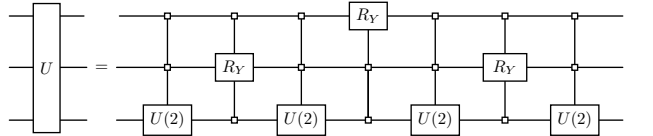
Appendix C: Recursive Cosine-Sine decomposition

Here, we review the optimized recursive cosine-sine decomposition (CSD) as introduced by Bergholm et al. in 2004 [19]. We aim to provide a modernized perspective on this decomposition, putting it into context with the flag decomposition in Eq. (6), and providing detailed computational instructions alongside an optimized implementation in just-in-time compilable Python code [30].

In App. C1, we begin with an overview of the circuit structure and gate counts without considering the details of the synthesis. Then we walk through the decomposition and optimization process in detail in App. C2. Finally, we provide some commentary on the mathematical structure of the recursive CSD and its relationship to the flag decomposition from the main text.

1. Overview of recursive CSD

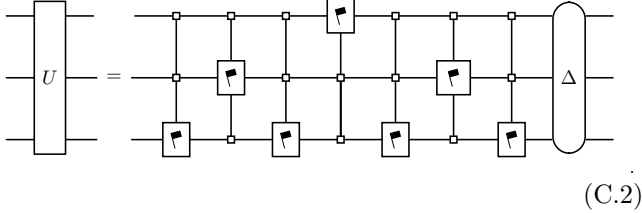
The CSD is a commonly used tool for matrix factorizations. It decomposes a unitary matrix U into two block-diagonal matrices and a block matrix of diagonals. The former can be decomposed recursively by applying CSDs to each subblock, while the block of diagonals is left intact. Showing the example of $n = 3$ qubits, this yields the circuit



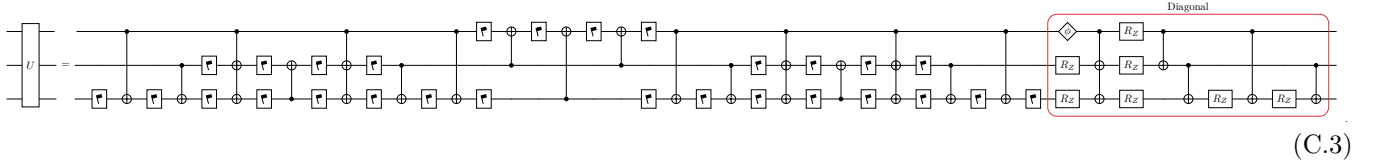
(C.1)

Here, we performed two recursion steps of the decomposition, and the multiplexed R_Y rotations implement the block matrix of diagonals. Afterwards, we perform a

“sweep” through the circuit, from left to right, in which we simultaneously decompose the multiplexers above into our target gate set and remove the overparametrization caused by the recursive CSD. If we are targeting a QROM architecture, we a) merge a diagonal from the left into a multiplexed $U(2)$ gate and decompose it, or b) split a diagonal into a part that is combined with a multiplexed R_Y rotation into a new multiplexed $U(2)$ gate, and a part that can be commuted through to the right. This leads to the following structure:



In this format, the synthesized circuit is particularly suited for the phase gradient decomposition; see



Doing this, we decomposed each of the $2^n - 1$ multiplexed flags into 2^{n-1} single-qubit flags and $2^{n-1} - 1$ CNOT gates. Further, we decomposed the diagonal into $2^n - 1$ R_Z rotations, $2^n - 2$ CNOT gates and a global phase ϕ (diamond shape); see App. D 4. This leads to total gate counts of

$$\begin{aligned} N_{\text{CNOT}}(n) &= (2^n - 1)(2^{n-1} - 1) + 2^n - 2 \\ &= \frac{1}{2}4^n - \frac{1}{2}2^n - 1, \end{aligned} \quad (\text{C.4})$$

$$\begin{aligned} N_{\text{rot}}(n) &= (2^n - 1)(2^{n-1} \cdot 2) + 2^n - 1 \\ &= 4^n - 1. \end{aligned} \quad (\text{C.5})$$

The rotation count matches the lower bound for $U(2^n)$ ²². The CNOT count is slightly above the best known count from the Block-ZXZ or QSD decompositions, and asymptotically a factor 2 larger than the lower bound. We were not able to find the opportunity to cancel one more CNOT that is being hinted at in [19], so we report a count that is larger by 1.

²² Note that we refer to the rotation gate count here, which is one less than the parameter count due to the global phase.

Sec. III A. It costs $2^n - 1$ multiplexed single-qubit flags with $n - 1$ multiplexing nodes each, and one n -qubit diagonal gate.

Alternatively, when targeting the gate set $\{R_Y, R_Z, \text{CNOT}\}$, the sweep can make use of a single step, treating multiplexed R_Y gates just like a multiplexed $U(2)$ gate. In this step, we decompose multiplexed $U(2)$ gates into a diagonal and (non-multiplexed) single-qubit flag circuits interleaved with CNOT gates. See App. C 2 for details on the sweeping steps.

We may choose the order of the multiplexing qubits between neighbouring multiplexers such that the synthesized circuit becomes a bit less sparse. In a last step, the diagonal obtained at the right end of the circuit can be decomposed into multiplexed R_Z rotations [38, 49], which in turn decompose into R_Z rotations and CNOT gates. For $n = 3$, we arrive at the following synthesized circuit for the gate set $\{R_Y, R_Z, \text{CNOT}\}$:

2. Instructions for CSD compilation

We now describe the recursive CSD compilation process in detail, aiming for a complete, comprehensive description that also serves as additional documentation for our implementation [30].

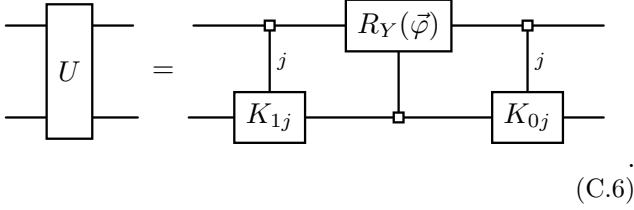
a. Recursive CSD decomposition

A CSD decomposes a $d \times d$ unitary matrix U into two block-diagonal unitary matrices $K_{0,1}$ and a 2×2 block matrix of real-valued diagonals whose squares sum to $2\mathbb{1}_d$:

$$\begin{aligned} U &= K_0 A K_1 = \begin{pmatrix} K_{00} & 0 \\ 0 & K_{01} \end{pmatrix} \begin{pmatrix} C & -S \\ S & C \end{pmatrix} \begin{pmatrix} K_{10} & 0 \\ 0 & K_{11} \end{pmatrix} \\ K_{ij} &\in \mathcal{U}(d/2) \\ C &= \text{diag}(\cos(\varphi_0), \dots, \cos(\varphi_{d/2})) \\ S &= \text{diag}(\sin(\varphi_0), \dots, \sin(\varphi_{d/2})). \end{aligned}$$

While the block sizes in K_0 and K_1 could differ in general, leading to a more fractured structure of A (see

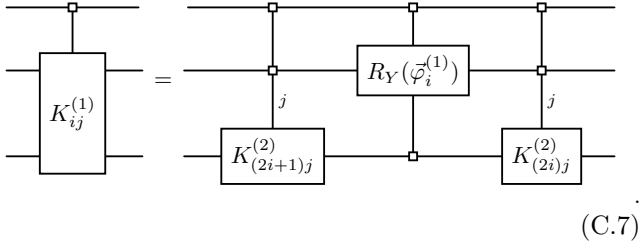
e.g. App. E2), we here limited ourselves to an even dimension d and a specific CSD that produces $d/2$ rotation angles $\vec{\varphi}$ and block matrices of size $d/2 \times d/2$. As we work with unitaries represented on qubits, we specifically set $d = 2^n$, and represent the CSD as a quantum circuit, c.f. Eq. (10):



(C.6)

The CSD is readily available in code via standard linear algebra libraries, such as `scipy` in Python [28]. Conveniently, we separately obtain the unitary matrix blocks K_{ij} and the angles $\vec{\varphi}$ ²³. In code, we represent each multiplexed unitary as a list of complex matrix blocks, or a complex 3-tensor, and each multiplexed R_Y gate as a vector storing the angles $\vec{\varphi}$ together with an integer denoting the target qubit index.

Next, we may apply the CSD to each of the two multiplexed unitaries, by applying it to each block separately and combining the results into two doubly-multiplexed unitaries on $n - 2$ qubits and one $n - 1$ -multiplexed R_Y rotation:



(C.7)

Here we denoted the recursion level with a superscript, so that $U = K_{00}^{(0)}$ for the input U and $K_{ij} = K_{ij}^{(1)}$ for the blocks from Eq. (C.6). These blocks in general have 5 indices; one for the recursion depth (superscript), one for the index of the multiplexed unitary at a given recursion depth (first subscript), the block index along the diagonal within a multiplexed unitary (second subscript), and finally the two indices into the matrix block itself (not printed explicitly). Note that the superscript has an effect on the range of all other indices and we only require the data from one recursion level to describe the full circuit. As such, the superscript can be seen as an index over time during the compilation process.

At recursion level r , a full circuit description consists of 2^r r -multiplexed $(n - r)$ -qubit unitaries (represented by one complex 3-tensor of shape $(2^r, 2^{n-r}, 2^{n-r})$ each) and $2^r - 1$ $(n - 1)$ -multiplexed R_Y rotations (a real vector of length 2^{n-1} and an integer, each). The total number of real parameters stored at this level is thus

$$2 \cdot 2^{r+r+2(n-r)} + (2^r - 1)2^{n-1} = 2 \cdot 4^n + (2^r - 1)2^{n-1}, \quad (\text{C.8})$$

where the overhead factor 2 in the leading term stems from the generic representation of unitary matrices as complex matrices, and the second term directly points at the overparametrization introduced during the recursive CSD.

At recursion level $r = n - 1$, we arrive at the circuit shown in Eq. (C.1), with an overparametrization of

$$4^{n-1} - 2^{n-1}, \quad (\text{C.9})$$

an overhead of about 25% over the 4^n parameters that uniquely determine U . The next step, which is concerned with removing these excess parameters and decomposing into a preferred gate set, depends on that target gate set. We describe it for a QROM-based architecture that directly uses Eq. (C.2) together with the implementation of multiplexed flags described in Sec. III A, and for the more traditional gate set $\{R_Y, R_Z, \text{CNOT}\}$ without using auxiliary qubits, arriving at Eq. (C.3).

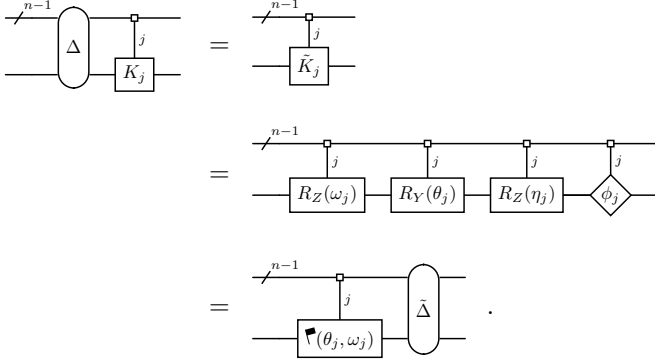
b. Phase gradient decomposition

If the target gate set consists of multiplexed flags and diagonals, we are almost at the desired circuit after performing the recursive CSD, but we still need to get rid of the massive overparametrization. For this, we will need two subroutines: pulling a diagonal unitary from left to right (in circuit ordering) through a multiplexed $U(2)$ gate while reducing it to a multiplexed flag, and pulling a diagonal unitary from left to right through a multiplexed R_Y rotation while *enhancing* it to a multiplexed flag²⁴.

The first subroutine is summarized as follows:

²³ In `scipy.linalg.cossin`, this is available via the setting `separate=True`.

²⁴ It is perfectly valid to invert the direction, which will result in multiplexed “right-handed” single-qubit flags.



We are given a diagonal unitary Δ and a $(n-1)$ -multiplexed $U(2)$ gate, represented as $2^{n-1} 2 \times 2$ matrices $\{K_j\}_j$, whose target we assume to be the least significant qubit. Then, we may first merge Δ into the multiplexer by computing $\tilde{K}_j = K_j \Delta_{[2j:2j+2]}$, interpreted as matrix multiplication. Next, we pull off a diagonal from the modified multiplexer to the right. Computationally, we do this by decomposing each of the $\{\tilde{K}_j\}_j$ into a global phase (diamond shape) and standard Euler angles:

$$\boxed{\tilde{K}_j} = \boxed{R_Z(\omega_j)} \boxed{R_Y(\theta_j)} \boxed{R_Z(\eta_j)} \diamond \phi_j,$$

grouping the resulting angles into vectors $\vec{\phi}$, $\vec{\eta}$, $\vec{\theta}$ and $\vec{\omega}$ of length 2^{n-1} , and processing the vectors $\vec{\eta}$ and $\vec{\phi}$ into the diagonal unitary

$$\tilde{\Delta} = e^{-i(\vec{\phi}+\vec{\eta}/2)} \oplus_{n-1} e^{-i(\vec{\phi}-\vec{\eta}/2)}. \quad (\text{C.10})$$

Here we introduced the notation \oplus_k to denote the direct sum between two equally-sized vectors rearranged such that the split of the total vector space corresponds to that arising from the split $|0\rangle \oplus |1\rangle$ on the k th out of all qubits (using zero-based indexing). We illustrate the notation with some examples:

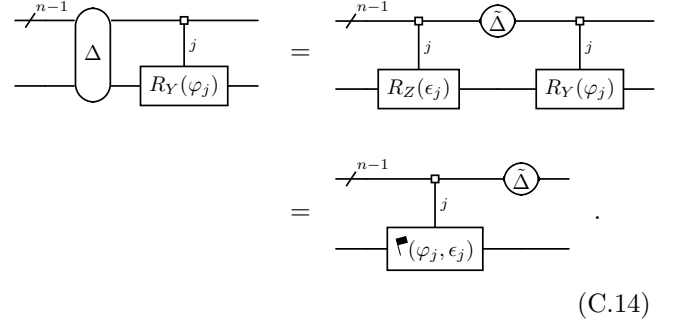
$$(a, b, c, d) \oplus_0 (e, f, g, h) = (a, b, c, d, e, f, g, h) \quad (\text{C.11})$$

$$(a, b, c, d) \oplus_1 (e, f, g, h) = (a, b, e, f, c, d, g, h) \quad (\text{C.12})$$

$$(a, b, c, d) \oplus_2 (e, f, g, h) = (a, e, b, f, c, g, d, h). \quad (\text{C.13})$$

The Euler decomposition can be computed in code with simple (inverse) trigonometric functions. We thus moved the diagonal unitary Δ through the multiplexer $\{K_j\}_j$, resulting in the modified diagonal unitary $\tilde{\Delta}$ and the multiplexed flag with angles $\vec{\omega}$ and $\vec{\theta}$ for its R_Z and R_Y rotations, respectively.

The second subroutine is summarized as follows:



$$(\text{C.14})$$

We are given a diagonal unitary Δ and a multiplexed R_Y gate, defined by 2^{n-1} angles $\vec{\varphi}$ and a target qubit index k . We split Δ into a diagonal on all qubits except the one with index k , and a $(n-1)$ -multiplexed R_Z rotation with target qubit index k . For this, we compute the complex arguments of Δ , and split them into two vectors $\vec{\delta}_{0,1}$ of length 2^{n-1} such that $\Delta =: e^{i\vec{\delta}_0} \oplus_k e^{i\vec{\delta}_1}$. We may rewrite this as

$$\Delta = e^{i\vec{\delta}_0} \oplus_k e^{i\vec{\delta}_1} \quad (\text{C.15})$$

$$= e^{i(\vec{\delta}_0+\vec{\delta}_1)/2} e^{i(\vec{\delta}_0-\vec{\delta}_1)/2} \oplus_k e^{i(\vec{\delta}_0+\vec{\delta}_1)/2} e^{-i(\vec{\delta}_0-\vec{\delta}_1)/2} \quad (\text{C.16})$$

$$= \left(e^{i(\vec{\delta}_0+\vec{\delta}_1)/2} \otimes_k (1,1) \right) \left(e^{i(\vec{\delta}_0-\vec{\delta}_1)/2} \otimes_k (1,-1) \right) \quad (\text{C.17})$$

$$=: \left(\tilde{\Delta} \otimes_k \mathbb{1}_2 \right) \text{MUX-}R_Z(\vec{\epsilon}, k), \quad (\text{C.18})$$

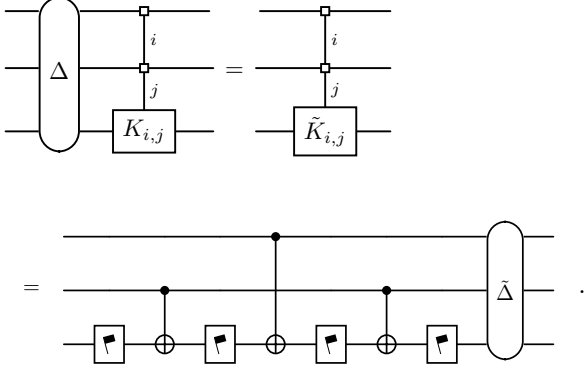
where we extended the subscript notation from \oplus to \otimes to denote a $((n-1) \otimes 1)$ -qubit tensor product with the single qubit at qubit index k . Now we may commute the diagonal $\tilde{\Delta}$ through the given R_Y multiplexer controls. In turn, this multiplexer combines with the R_Z multiplexer to form a multiplexed flag, completing the subroutine.

With the two subroutines in our hands, we simply sweep from left to right through the circuit obtained by the recursive CSD, applying the subroutines alternately. For the left-most multiplexer, there is no diagonal to merge from the left, so we start immediately with the Euler decomposition step of the first subroutine. After the sweep, we obtain the circuit in Eq. (C.2), which can then be compiled further into QROMs and adders, using auxiliary qubits and phase gradient states.

c. Auxiliary-free decomposition

For the classical gate set $\{R_Y, R_Z, \text{CNOT}\}$ and without auxiliary wires, we follow a similar strategy as for the QROM architecture, but we will directly integrate the decomposition of multiplexers with the reduction of the overparametrization. For this, we use a single subroutine that we then apply to both the multiplexed $U(2)$

gates and the multiplexed R_Y rotations alike. It proceeds as follows:



The subroutine compiles a diagonal unitary Δ followed by a given multiplexed $U(2)$ gate $\{K_j\}_j$ into single-qubit flags, CNOT gates, and a new diagonal $\tilde{\Delta}$. It was described first in [19]. If we are given a multiplexed R_Y gate, we simply replace it by a multiplexed $U(2)$ gate by converting the given vector of rotation angles into the respective sequence of 2×2 rotation matrices. In either case, we multiply the diagonal into the multiplexer via $\tilde{K}_j = K_j \Delta_{[2j:2j+2]}$, like for the first subroutine in the previous section.

The subroutine then exclusively consists of $U(2)$ *de-multiplexing*, a recursive technique to remove multiplexing nodes from a $U(2)$ gate until we arrive at a parameter-optimal circuit of single-qubit flags and an n -qubit diagonal. It can be considered the key innovation unlocking the reduced CNOT count in the optimized CSD decomposition [19]. Further details can also be found in the PennyLane compilation hub [41].

Let's first consider the simplest case of a single multiplexing node, which also serves as base case for the recursion. We de-multiplex a singly-multiplexed $U(2)$ operator $\{K_0, K_1\}$ with a variant of a type-A Cartan decomposition that is used for de-multiplexing larger operators. First, compute $X = K_0 K_1^\dagger$ ²⁵ and denote its matrix as

$$X = e^{i\phi/2} \begin{pmatrix} a & b \\ -\bar{b} & \bar{a} \end{pmatrix}. \quad (\text{C.19})$$

Then, define the angles

$$\rho_0 = \frac{\pi - \phi}{4} - \frac{\arg(a)}{2}, \quad (\text{C.20})$$

$$\rho_1 = \frac{3\pi - \phi}{4} + \frac{\arg(a)}{2}, \quad (\text{C.21})$$

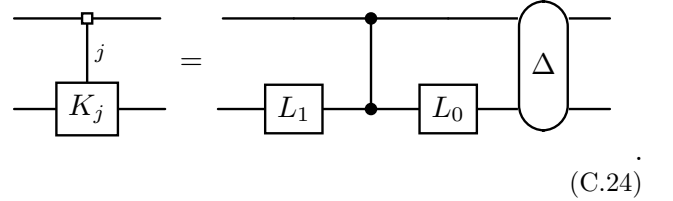
as well as the matrix $r = \text{diag}(e^{i\rho_0}, e^{i\rho_1})$ and compute $Y = rXr$. The eigenvalues of Y then are guaranteed to be $\pm i$, i.e.,

$$Y = L_0 \text{diag}(i, -i) L_0^\dagger \quad (\text{C.22})$$

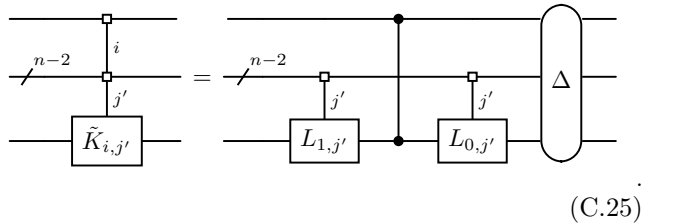
for a unitary L_0 . Finally, define $d = \text{diag}(e^{i\pi/4}, e^{-i\pi/4})$ and $L_1 = dL_0^\dagger r^\dagger K_1$. Then we have

$$\begin{aligned} K_1 &= r L_0 d^\dagger L_1 \\ K_0 &= r^\dagger Y r^\dagger K_1 = r^\dagger L_0 d^2 L_0^\dagger r^\dagger (r L_0 d^\dagger L_1) \\ &= r^\dagger L_0 d L_1 \\ \begin{pmatrix} K_0 & 0 \\ 0 & K_1 \end{pmatrix} &= \begin{pmatrix} r^\dagger & 0 \\ 0 & r \end{pmatrix} \begin{pmatrix} L_0 & 0 \\ 0 & L_0 \end{pmatrix} \begin{pmatrix} d & 0 \\ 0 & d^\dagger \end{pmatrix} \begin{pmatrix} L_1 & 0 \\ 0 & L_1 \end{pmatrix}. \end{aligned} \quad (\text{C.23})$$

That is, we decomposed the multiplexer into two single-qubit unitaries L_0 and L_1 , a static diagonal $D = d \oplus d^\dagger = \text{diag}(e^{i\pi/4}, e^{-i\pi/4}, e^{-i\pi/4}, e^{i\pi/4})$, and a diagonal matrix $R = r^\dagger \oplus r$ in the form of a multiplexed R_Z gate. We can polish this decomposition to suit our purposes by extracting from D an S^\dagger gate on each qubit as well as a global phase, and merging them into L_1 and R . We then obtain the circuit



For our case of multiple multiplexing qubits, we choose one of them and pair up the matrices of the multiplexer corresponding to the states $|0\rangle, |1\rangle$ of that qubit. For simplicity, we here choose the most significant multiplexing qubit and write the matrix pairs as $\{\tilde{K}_{0j'}, \tilde{K}_{1,j'}\}$. Then we apply the de-multiplexing above to each pair, arriving at the multiplexer-extended version of Eq. (C.24):



The $(n-2)$ -multiplexed $U(2)$ gate $\{L_{1,j'}\}$ is then de-multiplexed again, the resulting diagonal is merged into $\{L_{0,j'}\}$, and the latter is de-multiplexed as well. This way, we obtain a decomposition of $\{\tilde{K}_j\}$ into 2^{n-1} single-qubit $U(2)$ gates, $2^{n-1} - 1$ CZ gates, and a diagonal. At this point, we just need to reduce the parametrization

²⁵ This is almost the relative complex structure with respect to the relevant type-A Cartan involution, which is formed as $X \oplus X^\dagger$.

in this decomposition, which is highly redundant. For this, we start at the left of the circuit and decompose the $U(2)$ gate into a global phase and Euler rotations of the form $R_Z R_Y R_Z$. Then we merge the right R_Z gate through the CZ gate to its right into the next $U(2)$ gate, and the global phase into the trailing diagonal Δ . If CNOT gates are preferred over CZ gates, we can extract a Hadamard gate from the R_Y rotation to the left and from the $U(2)$ gate to the right of the CZ gate to transform it into a CNOT. This procedure is repeated, until we are left with 2^{n-1} single-qubit flags (R_Z followed by R_Y), $2^{n-1} - 1$ CZ (or CNOT) gates, and a diagonal. With this, we complete the subroutine of pulling a diagonal unitary through a multiplexed $U(2)$ gate while decomposing it into elementary gates at the same time.

The coarse-level compilation then proceeds exactly like for the QROM architecture: we repeatedly apply the subroutine to all multiplexers in Eq. (C.1), sweeping from left to right. This leaves behind the circuit shown in Eq. (C.3), which does not contain any excess parameters anymore.

3. Math commentary

The CSD of unitary (orthogonal) matrices is a KAK decomposition of type AIII (BDI) [50, 51], induced by a Cartan decomposition²⁶ of the corresponding Lie algebra $\mathfrak{u}(d)$ ($\mathfrak{so}(d)$). Cartan decompositions can be applied recursively, by further decomposing the subgroup \mathcal{K} from which the elements K in the KAK decomposition originate. This concept has been studied thoroughly in the past [9, 52–54]. For the unitary CSD, this subgroup of the total group $\mathcal{G} = U(d)$ is $\mathcal{K} = U(d/2) \times U(d/2)$, so that its elements K can be decomposed by applying CSDs to each factor individually. This structure manifests in the parallelized, or batched, decomposition of the blocks in the block diagonal matrices. The element A from the Abelian Cartan subgroup (CSG) \mathcal{A} , which corresponds to a maximal torus in the symmetric space $\mathcal{P} := \mathcal{G}/\mathcal{K}$, naturally takes the form of a multiplexed R_Y rotation for the conventional basis and involution choices, which in addition interacts favourably with the block diagonal structure of the subgroup(s). The CSG elements from higher recursion levels are just multiplexed R_Y rotations again, with the less significant multiplexer qubits originating in the higher-level CSD itself, and the more significant ones being inherited from the initial and intermediate K s. As reported in [9], a type-AIII decomposition (with dimensional parameters $p = q = d/2$) leads to an overparametrization of $d/2$. This matches the 2^{n-1} parameters in the R_Y multiplexer produced in the first CSD. Each recursion step has to decompose four times

as many matrices as the previous one, because there are twice as many subgroup elements, and each of them has an additional multiplexing node attached. Thus, the r th recursion step adds $2^{n-1}(\frac{1}{2})^{r-1}$ parameters. Summing up all added parameters, we find the same overparametrization count as in Eq. (C.9):

$$\sum_{r=1}^{n-1} 2^{n+r-2} = 2^{n-2}(2^n - 2) = 4^{n-1} - 2^{n-1}. \quad (\text{C.26})$$

Pulling a diagonal off a unitary matrix corresponds to the flag decomposition introduced in Eq. (6) in the main text, and it is the key step in the recursive CSD that allows us to remove the excess parametrization after the fact. As such, the flag decomposition allows us to exploit a particularly simple degree of freedom in KAK decompositions: elements from the commutant $\mathcal{K}^{\mathcal{A}}$ of the CSG \mathcal{A} within the subgroup \mathcal{K} can move freely between the two K s. For the first-level CSD with the standard choice of bases, we have

$$\mathcal{K}^{\mathcal{A}} = \exp(\text{span}_{i\mathbb{R}}\{\mathbb{1}_2 \otimes \{Z\}^{n-1}\}), \quad (\text{C.27})$$

i.e., the elements that can be merged through the R_Y multiplexer into the other group element are the $(n-1)$ -qubit diagonals obtained as part of the flag decomposition. Note that the diagonal group whose generators have a Pauli- Z on the first qubit instead are not part of the commutant. This emphasizes the compatibility between these two concepts, lifting the circuit decomposition technique by Bergholm et al. [19] to a mathematically founded technique that can readily be generalized to other Cartan decompositions. For example, in selective de-multiplexing, which we present in Sec. IV, the second step is a type-A Cartan decomposition of $U(d/2) \times U(d/2)$, which leads to an overparametrization of $d/2$. The CSG is $\mathcal{A} = \exp(\text{span}_{i\mathbb{R}}\{Z \otimes \{\mathbb{1}_2, Z\}^{n-1}\})$, the group of R_Z multiplexers targeting the most significant qubit. The commutant of this CSG within the subgroup $\mathbb{1}_2 \otimes U(d/2)$ is

$$\mathcal{K}^{\mathcal{A}} = \exp(\text{span}_{i\mathbb{R}}\{\mathbb{1}_2 \otimes \{Z\}^{n-1}\}), \quad (\text{C.28})$$

i.e., the (Abelian) group of diagonals acting on all but the most significant qubit. This is what allows us to leverage a flag decomposition into removing overparametrization, just like for the type-AIII Cartan decompositions above.

Flag decompositions thus form a useful additional tool when using Cartan decompositions in the context of parameter optimality, extending the very limited repertoire of *unique* (recursive) Cartan decompositions that do not introduce overparametrization at all [9].

Appendix D: Gate count calculations for {Clifford + Rot}

Here we present gate count calculations for important subroutines and gate families. We summarize them in Tab. II and collect comments for how to obtain those counts in the following.

²⁶ See [9] for some remarks about nomenclature and Abelian factors on top of semisimple algebras.

Subroutine	Rot	Clifford	Δ	comment
1Q-flag	2	0	0	Eq. (8)
2Q-flag	12	2	0	Eq. (9) [1]
mux_k -Rot	2^k	2^k	0	$k \geq 1$ [18]
sym-mux_k -Rot	2^k	$2^k - 1$	0	$k \geq 0$ [1]
mux_k -1Q-flag	2^{k+1}	$2^k - 1$	1	$k \geq 0$ [19]
mux_k -2Q-flag	$3 \cdot 2^{k+2}$	$6 \cdot 2^k - 4$	1	$k \geq 0$ Eq. (20)
n Q-flag	$4^n - 2^n$	$\frac{1}{2}4^n - \frac{3}{2}2^n + 1$	1	recursive flag decomp/CSD with $b = 1$; App. C, [19]
	$4^n - 2^n$	$\frac{1}{2}4^n - \frac{n+12}{8}2^n + 1$	1	$n \geq 3$
mux_k - n Q-flag	$(4^n - 2^n)2^k$	$\frac{1}{2}(4^n - 2^n)2^k - \frac{5}{4}2^n + 1$	1	$n \geq 2, k > 0$
n -qubit diagonal	$2^n - 1$	$2^n - 2$	0	
n -qubit unitary	$4^n - 1$	$\frac{1}{2}4^n - \frac{3}{8}(n+2)2^n + n - 1$	0	selective de-multiplexing
MPS prep	$(2L+1)4^n$	$\frac{1}{2}(2L+1)4^n - \frac{(2L+3)n+(8L+6)}{8}2^n + n - 1$	0	can be reduced further; App. E2

TABLE II: Gate counts for elementary subroutines used throughout this work, in the context of {Clifford + Rot} decompositions. The column Δ indicates whether an additional diagonal unitary is needed in the decomposition. All reported decompositions are parameter-optimal, except for parameters in the potentially required diagonal. We only report the cheapest decompositions, with an exception for the n -qubit flag for which we also show the cost by Bergholm et al., for comparison. See Sec. V for details about MPS state preparation.

1. One- and two-qubit flags

The one-qubit flag decomposition can be obtained from an Euler decomposition, as discussed in Eq. (8). The flag circuit consists of a single R_Z and a single R_Y gate.

The two-qubit flag decomposition, shown in Eq. (9), is reported in [1, Thm. 14] and [55, Prop. 10], without the mathematical context of flag manifolds. The flag circuit itself is given in terms of 2 CNOT gates and 12 Rot gates. Note that no diagonal is required for the flag circuit itself.

2. Multiplexed one- and two-qubit gates

mux_k -Rot A multiplexed Rot gate about the Pauli operator $P \neq X$ can be decomposed into an alternating sequence of CNOT and Rot gates [1, 40, 41]. For a single multiplexing node, there are 2 CNOT and two Rot gates, and their number doubles with each additional multiplexing node. This leads to 2^k CNOT and Rot gates each, for k multiplexing nodes. Note that this formula does not reproduce the cost of non-multiplexed rotations, as it predicts them to require a CNOT gate.

A slight generalization of the above, which allows us to treat R_X gates as well, is the decomposition of a multiplexed R_P gate, with P a Pauli word, into an alternating sequence of CQ and R_P gates, where Q is another Pauli word with $\{P, Q\} = 0$. This generalization holds because the only property of CNOT and R_Y (or R_Z) gates required for its derivation is the anti-commutativity between X and Y (or X and Z). For a given single-qubit operator P , there are only two options (up to an incon-

sequential phase) for anti-commuting single-qubit operators, say Q_0 and Q_1 . We then know the following decomposition, depicted for $n = 3$ for simplicity:

As a matter of fact, we can be even more flexible in the decomposition and choose the operator Q to differ at every location; for this, we pick the right-most Q_i to our liking, and create the decomposition in Eq. (D.1). Afterwards, we can use $R_P(\pm\frac{\pi}{2})Q_0R_P(\mp\frac{\pi}{2}) = Q_1$, where the sign choice depends on the assignment of the labels $Q_{0,1}$, to transform any of the other CQ_i into the alternative option. The inserted R_P gates are then simply absorbed into the present gates by modifying their angles. One example that we use in selective de-multiplexing in Sec. IV is the following decomposition:

The advantage of this flexibility is that we may adjust the decomposition of a multiplexed rotation such that the trailing (or leading, if preferred) entangling gate can

its k -multiplexed variant, is

$$C_{\text{CNOT}}^{\text{flag,D.6}}(n, k) = 2C_{\text{CNOT}}^{\text{flag}}(n-1, 1+k) \quad (\text{D.9})$$

$$+ C_{\text{CNOT}}^{\text{flag}}(1, n-1+k) \quad (\text{D.10})$$

where we denote the target and multiplexing qubit counts as arguments to C_{CNOT} . In contrast, Eq. (D.8) implies the cost relationship

$$C_{\text{CNOT}}^{\text{flag,D.8}}(n, k) = C_{\text{CNOT}}^{\text{flag}}(n-1, 1+k) \quad (\text{D.11})$$

$$+ 2C_{\text{CNOT}}^{\text{Rot}}(n-1+k) + 2C_{\text{CNOT}}^{\text{flag}}(n-1, k), \quad (\text{D.12})$$

where the multiplexed rotations are neighbouring suitable flags so that we may subtract one CNOT from their cost using the technique in Eq. (D.3), leading to

$$C_{\text{CNOT}}^{\text{Rot}}(k) = 2^k - 1. \quad (\text{D.13})$$

To settle which option is cheaper, we first inspect the cost at small qubit counts. For (k -multiplexed) two-qubit flags, we above found the optimal decomposition to contain $6 \cdot 2^k - 4$ CNOTs. With this, the cost to decompose a k -multiplexed 3-qubit flag is given by

$$C_{\text{CNOT}}^{\text{flag,D.6}}(3, k) = 2 \cdot (6 \cdot 2^{k+1} - 4) + (2^{k+2} - 1) \quad (\text{D.14})$$

$$= 28 \cdot 2^k - 9,$$

$$C_{\text{CNOT}}^{\text{flag,D.8}}(3, k) = 6 \cdot 2^{k+1} - 4 + 2(2^{k+2} - 1) + 2(6 \cdot 2^k - 4)$$

$$= 32 \cdot 2^k - 14,$$

where we used that k -multiplexed flags and (symmetrized) k -multiplexed Rot both cost $2^k - 1$ CNOTs. For non-multiplexed 3-qubit flags, we find the second option to be preferable, with a CNOT count of 18. In contrast, k -multiplexed 3-qubit flags are optimally decomposed with the first option, leading to $28 \cdot 2^k - 9$ CNOTs. This implies that when decomposing larger objects, we will choose a different strategy for 3-qubit flags and their multiplexed variant. We can combine their cost into

$$C_{\text{CNOT}}^{\text{flag,min}}(3, k) = 28 \cdot 2^k - 9 - \delta_{k0}. \quad (\text{D.15})$$

We can repeat this calculation for 4-qubit flags, and find

$$C_{\text{CNOT}}^{\text{flag,D.6}}(4, k) = 2 \cdot (28 \cdot 2^{k+1} - 9 - \delta_{k+1,0}) + (2^{k+3} - 1)$$

$$= 120 \cdot 2^k - 19, \quad (\text{D.16})$$

$$C_{\text{CNOT}}^{\text{flag,D.8}}(4, k) = (28 \cdot 2^{k+1} - 9 - \delta_{k+1,0}) + 2(2^{k+3} - 1)$$

$$+ 2 \cdot (28 \cdot 2^k - 9 - \delta_{k0})$$

$$= 128 \cdot 2^k - 29 - 2\delta_{k0}.$$

We find the same behaviour as for $n = 3$, with selective de-multiplexing being the better option for $k = 0$ only, where it saves 4 CNOTs. The coerced cost function is thus

$$C_{\text{CNOT}}^{\text{flag,min}}(4, k) = 120 \cdot 2^k - 19 - 4\delta_{k0}. \quad (\text{D.17})$$

At this point it seems wise to distill some recursion relations from the observed behaviour. Denote the minimized cost for a k -multiplexed n -qubit flag by

$$C_{\text{CNOT}}^{\text{flag,min}}(n, k) = A_n 2^k + B_n - C_n \delta_{k0}. \quad (\text{D.18})$$

We will prove by induction that $A_n = 2^{n-1}(2^n - 1)$, $B_n = 1 - 5 \cdot 2^{n-2}$ and $C_n = (n-2)2^{n-3}$. The induction hypothesis is that it holds for some n , which we have seen to be true for $n = 2$:

$$A_2 = 6 = 2 \cdot 3 = 2^{2-1}(2^2 - 1), \quad (\text{D.19})$$

$$B_2 = -4 = 1 - 5 = 1 - 5 \cdot 2^{2-2}, \quad (\text{D.20})$$

$$C_2 = 0 = (2-2)2^{2-3}. \quad (\text{D.21})$$

Then we make the induction step; for an $(n+1)$ -qubit flag, the two options yield the cost

$$C_{\text{CNOT}}^{\text{flag,D.6}}(n+1, k) = 2 \cdot (A_n 2^{k+1} + B_n - C_n \delta_{k+1,0})$$

$$+ (2^{k+n} - 1) \quad (\text{D.22})$$

$$= (4(2^{n-1}(2^n - 1)) + 2^n) 2^k$$

$$+ (2(1 - 5 \cdot 2^{n-2}) - 1)$$

$$= 2^n(2^{n+1} - 1) 2^k + (1 - 5 \cdot 2^{n-1}),$$

$$C_{\text{CNOT}}^{\text{flag,D.8}}(n+1, k) = (A_n 2^{k+1} + B_n - C_n \delta_{k+1,0})$$

$$+ 2(2^{k+n} - 1)$$

$$+ 2 \cdot (A_n 2^k + B_n - C_n \delta_{k0})$$

$$= (4(2^{n-1}(2^n - 1)) + 2^{n+1}) 2^k$$

$$+ (3(1 - 5 \cdot 2^{n-2}) - 2)$$

$$- 2(n-2)2^{n-3} \delta_{k0}$$

$$= 2^{2n+1+k} + (1 - 15 \cdot 2^{n-2})$$

$$- (n-2)2^{n-2} \delta_{k0}.$$

Here we used the induction hypothesis to fill in A_n, B_n and C_n . The second option has additional cost over the first of

$$2^{n+k} - \left(\frac{15}{4} - \frac{5}{2}\right) 2^n - (n-2)2^{n-2} \delta_{k0} \quad (\text{D.23})$$

$$= \begin{cases} -\frac{n-1}{4} 2^n & k = 0 \\ 2^n(2^k - \frac{5}{4}) & k > 0 \end{cases}, \quad (\text{D.24})$$

such that it is cheaper for $k = 0$ and more expensive for $k > 0$. This means that the minimized cost for the $(n+1)$ -qubit flag is given by

$$2^n(2^{n+1} - 1) 2^k + (1 - 5 \cdot 2^{n-1}) - (n-1)2^{n-2} \delta_{k0}, \quad (\text{D.25})$$

which is exactly the statement of the induction for $n+1$.

We thus may conclude for all n that the selective de-multiplexing step is favourable for non-multiplexed n -qubit flags, and the recursive flag decomposition/CSD

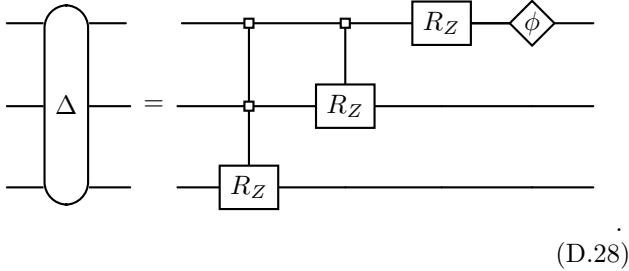
step is preferable for multiplexed flags, with the final CNOT cost

$$C_{\text{CNOT}}^{\text{flag}}(n) = \frac{1}{2}4^n - \frac{n+12}{8}2^n + 1, \quad (\text{D.26})$$

$$C_{\text{CNOT}}^{\text{mux-flag}}(n, k) = \frac{1}{2}(4^n - 2^n)2^k - \frac{5}{4}2^n + 1. \quad (\text{D.27})$$

4. Diagonal unitaries

A diagonal unitary can be decomposed into a sequence of (multiplexed) R_Z rotations and a global phase, denoted by a diamond-shaped gate, by iterating Eq. (13):



(D.28)

As we noted above, a k -multiplexed R_Z rotation requires 2^k CNOT gates, and for each of $1 \leq k \leq n-1$ we get one multiplexer, so that the diagonal in total costs

$$C_{\text{CNOT}}^{\text{diag}}(n) = \sum_{k=1}^{n-1} 2^k = 2^n - 2. \quad (\text{D.29})$$

5. Arbitrary unitaries

We may now compute the CNOT cost of a unitary. At the first level, we can choose between no de-multiplexing (pure CSD, Eq. (18)), selective de-multiplexing (Eq. (31)), and full de-multiplexing (QSD, Eq. (30)). This results in the cost

$$\begin{aligned} C_{\text{CNOT}}^{U, \text{CSD}}(n) &= 2C_{\text{CNOT}}^{\text{mux-flag}}(n-1, 1) \\ &\quad + C_{\text{CNOT}}^{\text{mux-flag}}(1, n-1) + C_{\text{CNOT}}^{\text{diag}}(n) \\ &= \frac{1}{2}4^n - \frac{3}{4}2^n - 1, \end{aligned} \quad (\text{D.30})$$

$$\begin{aligned} C_{\text{CNOT}}^{U, \text{selective}}(n) &= 2C_{\text{CNOT}}^{\text{flag}}(n-1) + 2C_{\text{CNOT}}^{\text{sym-mux-Rot}}(n-1) \\ &\quad + C_{\text{CNOT}}^{\text{mux-flag}}(n-1, 1) + C_{\text{CNOT}}^{\text{diag}}(n) \\ &= \frac{1}{2}4^n - \frac{n+4}{8}2^n - 1, \end{aligned} \quad (\text{D.31})$$

$$\begin{aligned} C_{\text{CNOT}}^{U, \text{QSD}}(n) &= 3C_{\text{CNOT}}^{\text{flag}}(n-1) + 2C_{\text{CNOT}}^{\text{sym-mux-Rot}}(n-1) \\ &\quad + C_{\text{CNOT}}^{\text{mux-Rot}}(n-1) + C_{\text{CNOT}}^U(n-1). \end{aligned} \quad (\text{D.32})$$

Here, we used the results of the previous sections and employed the reduction of the cost of multiplexed rotations by one where appropriate, according to Sec. IV

and Eq. (28) in particular. Note that the relations use the decomposition of (multiplexed) flags that come with constraints of $n \geq 3$ ($n \geq 2$). For the QSD step, we do not have the explicit cost yet. However, we can compute the difference between the selective de-multiplexing and QSD, and by bounding $C_{\text{CNOT}}^U(n-1)$ using the cost with selective de-multiplexing itself, we find that QSD will perform better in general. This tells us that unitaries should be de-multiplexed fully, which was not possible in a parameter-optimal way for flag circuits in the previous section. For three qubits, we reproduce the best known CNOT count of 19 through our techniques:

$$C_{\text{CNOT}}^{U, \text{SDM}}(3) = 3 \cdot 2 + 2(2^2 - 1) + 2^2 + 3 = 19, \quad (\text{D.33})$$

where we used that a two-qubit flag (unitary) costs 2 (3) CNOTs and that two of the multiplexed rotations can be implemented at reduced cost due to the trick in Eq. (28).

In order to generalize, we need to resolve the recursion relation

$$\begin{aligned} A(n) &= 3C_{\text{CNOT}}^{\text{flag}}(n-1) + 2C_{\text{CNOT}}^{\text{sym-mux-Rot}}(n-1) \\ &\quad + C_{\text{CNOT}}^{\text{mux-Rot}}(n-1) + A(n-1) \end{aligned} \quad (\text{D.34})$$

$$= \frac{3}{8}4^n - \frac{3}{16}(n+3)2^n + 1 + A(n-1), \quad (\text{D.35})$$

with the base case $A(3) = 19$ for three qubits. The solution is

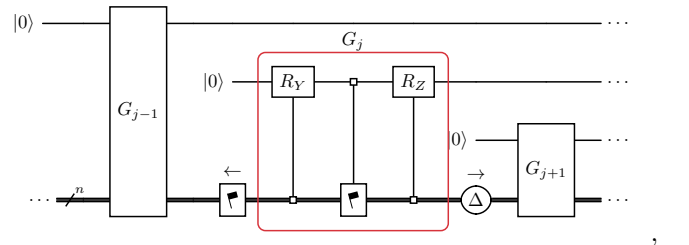
$$C_{\text{CNOT}}^{U, \text{SDM}}(n) = \frac{1}{2}4^n - \frac{3}{8}(n+2)2^n + n - 1. \quad (\text{D.36})$$

Although we derived it for $n \geq 3$, it turns out that this formula also conveniently reproduces the value for $n = 2$, which is 3, correctly.

Appendix E: Details for MPS preparation

1. Causal ordering for practical synthesis

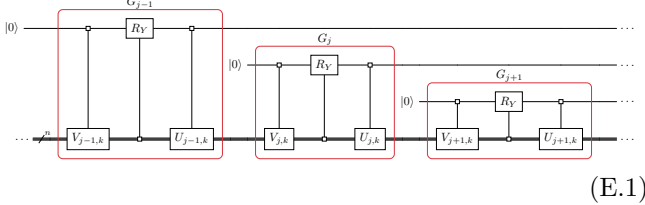
In order to compensate for the gauge degrees of freedom in Sec. VB, we set out to merge the n -qubit flag \blacktriangledown and diagonal Δ to the left and right, respectively. In particular, in Eq. (45), we want to perform



where the arrows above \blacktriangledown and Δ indicate the merge direction. However, this means that in order to synthesize G_j , we already need to have merged the flag circuit from G_{j+1} into G_j . In order to achieve this in practice, we

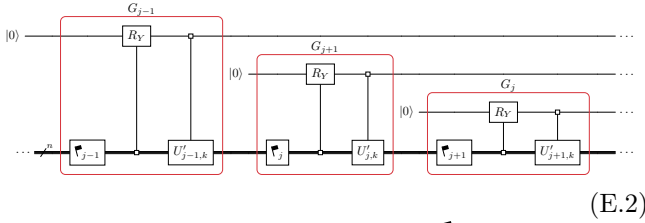
need to be careful about the causal order in which we synthesize the matrices. We will walk through the synthesis step by step in the following.

First, we synthesize each matrix G_j in an over-parametrized fashion by performing a standard CSD:



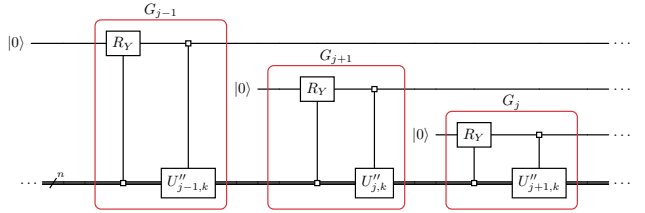
(E.1)

The index $k \in \{0,1\}$ indicates the two possible values from the single-qubit multiplexing. We then simply remove the multiplexer node attached to the V matrices, flag-decompose the resulting $V = \Delta \blacktriangleright^{29}$, and merge the diagonal Δ into the multiplexed U on the right, yielding $U' := U \cdot \Delta$:



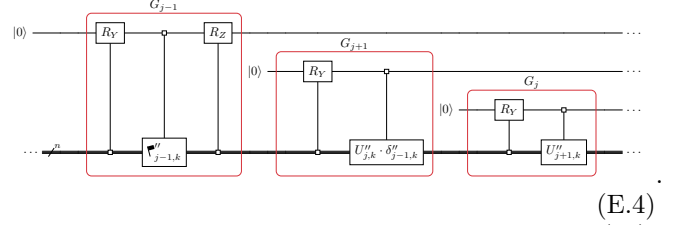
(E.2)

In the next step, we merge all leading \blacktriangleright_j unitaries in the previous multiplexed $U_{j-1,k}$, yielding $U''_{j,k} := U_{j,k} \blacktriangleright_{j+1}$:



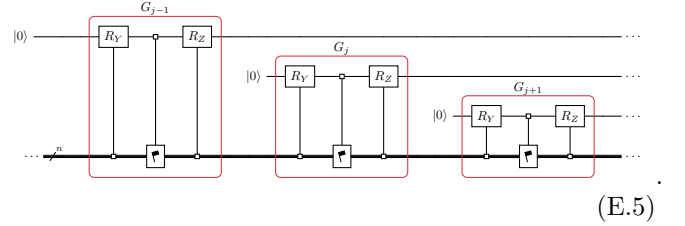
(E.3)

Up until this point, everything could be performed in parallel. Now we need to be careful with the causal ordering, moving from left to right in the chain of isometries G_j . We flag-decompose the first multiplexed unitary $U''_{0,k} = \Delta'' \blacktriangleright$. The diagonal Δ'' is then decomposed into a multiplexed R_Z and a smaller diagonal δ'' . This smaller diagonal is then merged with the multiplexed unitary $U''_{1,k}$ on the right. This is sequentially repeated going from left to right in the MPS:



(E.4)

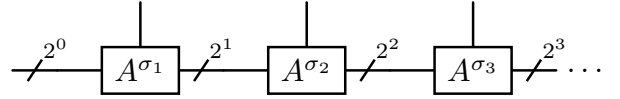
Finally, we reach the desired circuit structure of Eq. (46), where each isometry is parameter-optimal,



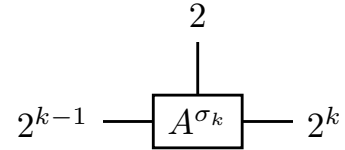
(E.5)

2. Boundary effect savings in MPS preparation

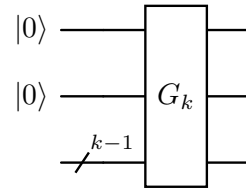
The dimensions of MPS tensors at the boundary are growing in steps of 2 at each site:



In general, the isometry A^{σ_k} has dimensions $2^{k-1} \times 2 \times 2^k$,



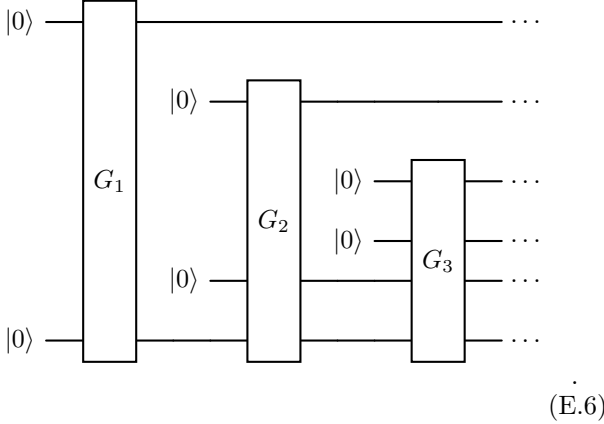
The corresponding unitary completion G_k maps from $k-1$ qubits to $k+1$ qubits, where the reduced input is due to the reduced dimension 2^{k-1} for the left horizontal bond:



Note that this argument can be reversed for the right boundary, with the isometries being such that they produce $|0\rangle$ states.

²⁹ Keep in mind that the ordering of matrix multiplication is reversed compared to the circuit diagrams.

Starting from the left boundary, we obtain a circuit structure where a new zeroed qubit is added at the top and then left untouched, and a new zeroed qubit is added for each isometry to the lower qubit register:



This is continued until the maximal bond dimension $\chi = 2^n$ is reached. In particular, we go from $k = 1$ until n . The isometries G_k at the boundary live in a Stiefel manifold of dimension $2(2^{k-1}) \times (2^{k+1}) - (2^{k-1})^2 = \frac{7}{4} \chi_k^2$, where we define $\chi_k = 2^k$ as the local bond dimension. We now need to construct a circuit for G_k that attains this optimal parameter bound. Additionally, we remove the extra $4^{k-1} = \frac{1}{4} \chi_k^2$ gauge degrees of freedom between site $k-1$ and k . Thus, we overall need to attain the *optimal* bound on the degrees of freedom (DOF),

$$C_{\text{DOF}} = \frac{6}{4} \chi_k^2. \quad (\text{E.7})$$

Simply repeating the trick from Eq. (43) does not suffice as it leads to $\frac{10}{4} \chi_k^2$ degrees of freedom. We need a better first decomposition to account for the **two** zeroed inputs. This is achieved by a CSD that allows for differently shaped blocks on either side of the central multiplexer. Concretely, we compute the decomposition

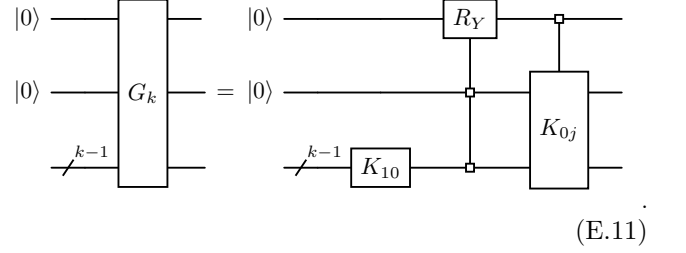
$$G_k = \begin{pmatrix} K_{00} & \mathbf{0} \\ \mathbf{0} & K_{01} \end{pmatrix} A \begin{pmatrix} K_{10} & \mathbf{0} \\ \mathbf{0} & K_{11} \end{pmatrix}. \quad (\text{E.8})$$

The dimensions are chosen such that $K_{10} \in U(2^k)$, $K_{11} \in U(3 \cdot 2^k)$ and $K_{0j} \in U(2 \cdot 2^k)$. The A can be chosen to be an R_Y multiplexer as in the regular CSD³⁰. Now, choosing the two zeroed qubits to be the most significant bits, we write the input quantum state as $|00\rangle \otimes |\psi\rangle$ and find the asymmetrically multiplexed gate $K_{10} \oplus K_{11}$ to act on it as

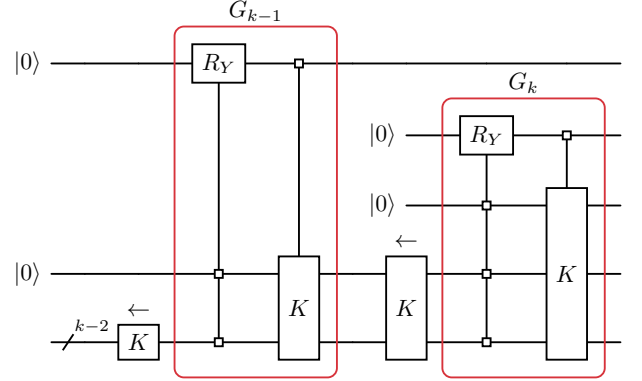
$$(K_{10} \oplus K_{11})(|00\rangle \otimes |\psi\rangle) = (K_{10} \oplus K_{11})(|\psi\rangle \oplus |0_{3 \cdot 2^k}\rangle) \quad (\text{E.9})$$

$$= |00\rangle \otimes (K_{10}|\psi\rangle). \quad (\text{E.10})$$

That is, K_{11} does not have any impact on the state, and we may as well change it, for example to $K_{10}^{\oplus 3}$. This replaces the asymmetric multiplexer by the gate $\mathbb{1}_4 \otimes K_{10}$.

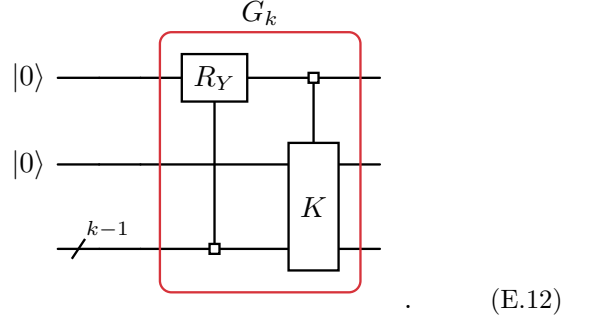


At this stage, it is easy to see how we can remove the $4^{k-1} = \frac{1}{4} \chi_k^2$ gauge degrees of freedom: We simply merge the unitary of exactly this size with the unitary of the same size that is multiplexed on the top qubit (indicated by arrows):



Note that in this diagram we left out the subscripts for the sake of brevity.

Next, we may use the second zeroed qubit to remove the corresponding multiplexing node of the R_Y gate, to obtain

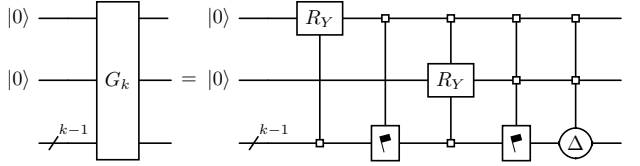


The multiplexed unitary K can be either de-multiplexed and then flag-decomposed when targeting the {Clifford + Rot} gate set, or directly flag-decomposed when targeting phase gradient decompositions. The steps are analogous to Sec. VA and Sec. VB, respectively. Let us walk

³⁰ Half of the angles in this multiplexer take a special value, but this will not be too relevant for us.

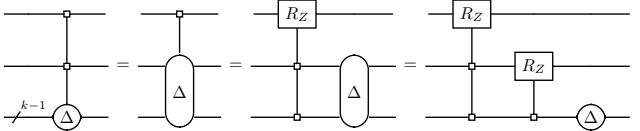
through the former explicitly to make sure we have the right number of parameters.

In particular, after flag-decomposing the multiplexed K_{0j} we obtain



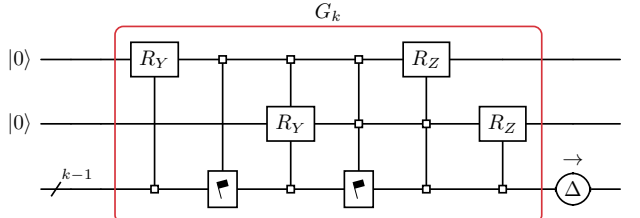
(E.13)

Note that we have removed another multiplexer on the second qubit, as well as the leading R_Z rotation due to the fixed input state (using the same argument as in Eq. (40)). We can then combine Eqs. (13) and (16) to yield the identity



(E.14)

With this we arrive at the final circuit for the boundary isometries



(E.15)

where the diagonal on the right can be again merged with the following isometry (as discussed in detail in the previous section).

The number of parameters in this circuit is composed of (from left to right)

$$\begin{aligned}
 C_{\text{DOF}} &= 2^{k-1} \text{ (multiplexed } R_Y) \\
 &\quad + 2(4^{k-1} - 2^{k-1}) \text{ (multiplexed flag)} \\
 &\quad + 2^k \text{ (multiplexed } R_Y) \\
 &\quad + 4(4^{k-1} - 2^{k-1}) \text{ (multiplexed flag)} \\
 &\quad + 2^k \text{ (multiplexed } R_Z) \\
 &\quad + 2^{k-1} \text{ (multiplexed } R_Z) \\
 &= \frac{6}{4}4^k = \frac{6}{4}\chi_k^2,
 \end{aligned}$$

matching the desired optimum from Eq. (E.7).